Hans Joakim Skadsem

Transport and Magnetisation Dynamics in Ferromagnetic Nanostructures

Thesis for the degree of Philosophiae Doctor

Trondheim, November 2009

Norwegian University of Science and Technology
Faculty of Natural Sciences and Technology
Department of Physics

NTNU
Norwegian University of
Science and Technology

NTNU
Norwegian University of Science and Technology

Thesis for the degree of Philosophiae Doctor

Faculty of Natural Sciences and Technology
Department of Physics

ISBN 978-82-471-1782-8 (printed version)
ISBN 978-82-471-1783-5 (electronic version)
ISSN 1503-8181

Doctoral theses at NTNU, 2009:192

Printed by NTNU-trykk

Abstract

We study transport and magnetisation dynamics in nanoscale ferromagnets and ferromagnetic heterostructures. Motivated by its novel physics and significant technological and commercial potential, we devote our attention to how the magnetisation in ferromagnets is affected by spin-flip scattering and applied currents. We also study the opposite effect, namely how the precessing magnetisation generates a spin current in a ferromagnet-superconductor heterostructure.

Excitations of the magnetisation vector are generated by *e.g.* external magnetic fields or spin currents traversing the ferromagnet. Spin dephasing mechanisms, such as scattering from magnetic impurities or the spin-orbit interaction, imply a loss of angular momentum. Unless the magnetic excitation is sustained by an external source, the magnetisation vector undergoes damped precessional motion towards a stable fixed point. We contribute to the understanding of magnetic dissipation by studying how the mentioned spin dephasing mechanisms affect the time evolution of the magnetisation vector in a uniform ferromagnet.

In inhomogeneous ferromagnets, such as domain walls, several intriguing effects caused by the interaction between current and magnetisation vector can be observed. Since the magnetisation varies in space, electrons flowing through the ferromagnet need to constantly adapt their spin direction to the varying magnetic configuration. Spin dephasing results in a mismatch between itinerant spins and the magnetisation. Mistracking generates current-driven magnetisation dynamics, which affects the magnetisation shape and position. We report analytical calculations of current-driven dynamics in itinerant ferromagnets and analyse numerical results obtained for ferromagnetic semiconductors.

The spin pumping effect, where a time-dependent magnetisation generates spin currents in neighbouring materials, has been studied extensively in normal metal-ferromagnet nanostructures. Using sophisticated fabrication techniques, heterostructures with both superconducting and ferromagnetic elements can now be manufactured. Inspired by spin pumping theory and recent interest in the superconducting proximity effect, we calculate charge and spin currents pumped by the magnetisation vector in a normal metal-ferromagnet-superconductor junction. We expand upon previous studies by considering pumping in the presence of applied bias voltage, and obtain results that coincide with expectations based on the spin valve pumping theory. The findings agree qualitatively with previous results in the absence of applied voltage.

Preface

This thesis is submitted to the Norwegian University of Science and Technology (NTNU) for partial fulfilment of the requirements for the degree of philosophiae doctor. The thesis is based on four papers which are related to magnetisation dynamics and the interplay between ferromagnetism and superconductivity in mesoscopic heterostructures.

The study has been performed at the Department of Physics, NTNU, Trondheim, between Autumn 2005 and Autumn 2009, with Professor Arne Brataas as supervisor. The work was financed by the Research Council of Norway through Grant No. 158547/431.

Trondheim, September 10, 2009

Hans Joakim Skadsem

List of papers

Paper [1]
Yaroslav Tserkovnyak, Hans Joakim Skadsem, Arne Brataas, Gerrit E. W. Bauer
"Current-induced magnetization dynamics in disordered itinerant ferromagnets"
Phys. Rev. B **74**, 144405 (2006)

Paper [2]
Hans Joakim Skadsem, Yaroslav Tserkovnyak, Arne Brataas, Gerrit E. W. Bauer
"Magnetization damping in a local-density approximation"
Phys. Rev. B **75**, 094416 (2007)

Paper [3]
Anh Kiet Nguyen, Hans Joakim Skadsem, Arne Brataas
"Giant Current-Driven Domain Wall Mobility in (Ga,Mn)As"
Phys. Rev. Lett. **98**, 146602 (2007)

Paper [4]
Hans Joakim Skadsem, Arne Brataas, Jan Martinek, Yaroslav Tserkovnyak
"FMR and voltage induced transport in normal metal–ferromagnet–superconductor trilayers"
Manuscript to be submitted to Phys. Rev. B (2009)

Contribution to the papers

I have contributed substantially to all parts of the two papers where I am listed as the first author, *i.e.* papers [2] and [4]. Analytical calculations, and in the case of paper [4] also numerical calculations, have been performed by me, and I am the main author of the text in both manuscripts. I performed unpublished calculations that significantly aided our understanding of the results in paper [1], and I worked on improving the original text of the manuscript. I developed part of the numerical code pertaining to magnetisation dynamics and helped in formulating the text of paper [3]. The model formulation, simulations and interpretation of results is mainly the work of the first author.

Contents

List of figures

Chapter 1

Introduction

Just over four decades ago, Neil Armstrong and Buzz Aldrin landed the lunar module *Eagle* in the south-western corner of the lunar plane Mare Tranquillitatis, or the Sea of Tranquility. The landing, at Tranquility Base on July 20th 1969, marked the definitive apex of the space race, and stands as a solid testament to the radical technological progress that had been achieved since President Kennedy declared *"We choose to go to the Moon"* in 1962. Families gathered around television sets, marvelling at the blurred pictures of Armstrong and Aldrin, the first men to leave their bootprints on the dry lunar surface, is a poignant symbol of mankind's long fascination with the Moon. As the only heavenly body close enough to Earth to sport features visible to the naked eye, the Moon continues to be a constant source of inspiration for practitioners in the fields of art, literature, science, music and philosophy.

The Moon and the Earth, one silently orbiting the other, is a prime example of what is referred to as the two-body problem in physics. A two-body problem is special in the sense that it can be transformed to two independent one-body problems, and thus often solved exactly. Once a third body is included, *e.g.* that of a weather satellite or an abandoned space vehicle, exact analytic solutions are usually out of reach. This observation is not restricted to satellites and lunar orbits, however, but is also valid for systems at the very opposite end of the scale, such as the hydrogen atom and the other elements of the periodic table.

The hydrogen atom, in which an electron moves around a proton, belongs to the somewhat mind-boggling realm of quantum mechanics, and not the classical world of celestial objects. The exact description of the hydrogen atom is found in most elementary textbooks on quantum mechanics, and provide a nice, albeit temporary, boost of morale for the reader. At one time or another, but most likely when ambitious studies of other elements in the periodic table are undertaken, the search for exact, microscopic solutions seems futile. Heads bang against walls anew, just as they did while working on that impossible many-body homework problem from an astrophysics class the previous semester. Feeling stumped already by helium, what then about 12 grams of the ^{12}C isotope, containing some $6{,}022 \cdot 10^{23}$ atoms? Thankfully, the detailed behaviour of each single electron is usually not what we

desire. The physical properties of the system at large is usually far more interesting, and as long as we stick to these, tremendous headway can still be achieved.

The Moon orbiting the Earth is in many ways an appealing analogy to the electron circling the proton in a hydrogen atom. The resemblance seems to suggest some underlying order or universality to Nature, which the rationalising brain fancy. To the dismay of some, perhaps, the analogy is not necessarily a good one, as certain pitfalls need circumnavigation when classical systems are scaled down into the world of quantum mechanics. A common example of an "issue" that might be encountered, is one that is seen when a magnetic moment traverses an inhomogeneous magnetic field, as in the pivotal Stern-Gerlach experiment. The experiment, which was devised in 1921 by Otto Stern and performed the following year together with Walther Gerlach, investigated how a beam of silver atoms is deflected as it passes through an inhomogeneous magnetic field [5]. Where none was expected, a vertical deflection parallel or anti-parallel to the gradient of the magnetic field was observed. The same two-fold beam splitting was observed when ground state hydrogen atoms was passed through an inhomogeneous magnet in a similar experiment a few years later [6]. These observations suggested the existence of an angular momentum unknown to classical physics, and unexpected at the time of the first Stern-Gerlach experiment.

During the years separating the two Stern-Gerlach measurements, the Dutch-American physicists Samuel A. Goudsmit and George E. Uhlenbeck made the radical suggestion that the electron has an *internal* angular momentum, a *spin*, that does not have a classical counterpart [7]. Being quantised and taking one of two values, *i.e.* either "up" or "down", the existence of electron spin offered an elegant, albeit unexpected, way out of the conundrum of the Stern-Gerlach experiments. Final evidence of the existence of spin came in the form of Paul A. M. Dirac's celebrated relativistic treatment of the Schrödinger equation, which confirmed Goudsmit and Uhlenbeck's hypothesis [8]. Thus, spin, being an integral part of quantum mechanics, follows directly from Dirac's wave equation, and is a particle property with no direct counterpart in the world of classical physics. As we will see, spin is not just an abstract concept, but a particle property that can be detected, manipulated and exploited to great advantage in modern technology.

Quantum mechanics, developed at furious pace during the first decades of the 20th century, was a great leap forward for the natural sciences. The emerging theory not only explained experiments and illustrated the limited applicability of classical theories, it also opened doors to rich, unprecedented physics. Lasers, nuclear power plants, transistors, modern chemistry, hard drives and flash memory chips are all founded upon our understanding of quantum theory. The idea of quantum computation or quantum teleportation, both active research areas, might tickle the fascination and interest of many, perhaps even those who derided natural sciences during their high school years.

A recent addition to our shared vocabulary is the concept of nanotechnology, a broad field in modern science and technology that is receiving extensive media coverage and ever increasing attention from scientists. As the name suggests, the main focus of nanotechnology is to develop, manufacture and efficiently utilise nano-scale

devices, ranging from nanopores used in hydrogen storage to gold nanoparticles that detect DNA sequences and clever nanofibres that make clothing wrinkle-free. As device sizes shrink, the importance of quantum phenomena increase, and one is forced to incorporate elements of quantum theory in a proper description of new implementations. Nanoelectronics is a direction within nanotechnology that seeks to combine elements of quantum theory with modern electronics, all in a push to improve our present day electronic devices. Combining "orthodox" electronic circuitry that are largely based on flow of electronic charge, with the electron spin, as in magnetoelectronics, is a very intriguing way of increasing functionality and performance of electronic devices. This thesis is devoted to theoretical studies of spin-dependent phenomena in nano-scale structures, and fits into the area of magnetoelectronics. In the following chapters and in the appended papers, we study dynamics of the magnetic order parameter in bulk ferromagnets, and how flow of spins affects, and is affected by, the magnetisation. The ambition of the thesis work has been to contribute to the present understanding of magnetisation dynamics at the nano-scale, and bring about results that might guide future developments in the field.

The thesis itself is based on four papers. My intention with the first part of the thesis is to give a general introduction the appended papers, without restating or repeating calculations. It is my hope that the papers themselves communicate these details. More space is granted to explaining the theoretical framework of paper [4] compared to the other three manuscripts. I believe the explicit results of this final paper require more technical background in order to be comprehensible, and I also think that more of the theoretical framework should be provided since the work is still unpublished.

Papers [1, 2, 3] are concerned with magnetisation dynamics in bulk ferromagnets, and how loss of angular momentum and how currents affect the time evolution of the magnetisation. Spin-flip scattering, such as magnetic impurity or extrinsic spin-orbit scattering, contributes to the loss of angular momentum, as these scattering processes randomise the electron spin. Such dissipative mechanisms ensure that the magnetisation move towards a stable fixed point, or a magnetic configuration corresponding to an energy minima.

Highly intriguing phenomena occur when a current is passed through an inhomogeneous ferromagnet. As current-carrying electrons traverse a magnetisation that varies in space, their spin try to align with the local magnetisation direction. Spin-flip scattering mechanisms randomise current-carrying spins, and this yields a mismatch between local magnetisation vector and itinerant spins. The mismatch results in an important current-induced torque that is capable of changing both the profile and the centre position of the magnetisation texture. Dissipation and this current-induced torque, both commonly quantified by phenomenological parameters in the magnetic equation of motion, and their relationship, is the topic of paper [1]. The follow-up study presented in paper [2] focuses on magnetic dissipation only, but should still be of interest since it clarifies subtle discrepancies between paper [1] and related contemporary studies of current-induced torques, *e.g.* Refs. [9, 10]. Paper [3] presents a numerical study of the effect of the current-induced torque in a ferromag-

netic semiconductor, with emphasis on how the intrinsic spin-orbit interaction in such materials affects the domain wall mobility. Finally, paper [4] is an analytical study of how a moving magnetisation in a uniform ferromagnet pumps spin into neighbouring materials, and in particular how a superconductor affects the pumped currents in a normal metal-ferromagnet-superconductor junction.

The organisation of the thesis is largely based on the content of the papers. An introductory review of magnetoelectronics and of superconductivity is given in the following chapter. In Chap. 3, emphasis is put on magnetisation dynamics, Gilbert damping and current-induced torque in bulk ferromagnets. Chap. 4 is devoted to the proximity effect in ferromagnet-superconductor junctions, and our calculation of pumped currents using a time-dependent scattering matrix formalism. The papers are appended after the bibliography.

Chapter 2

Preliminary concepts

The Greek word *meso* means "in between" or "intermediate". Physics observed on length scales *in between* the macroscopic and the microscopic worlds, belong to the class aptly titled mesoscopic physics. Devising a proper theoretical description of structures belonging to the class of mesoscopic objects can often be highly challenging. Devices that typically extend from a few atomic radii to a few microns are usually too complex to be studied by methods from the microscopic divide, and at the same time too small to be described by classical physics of the macroscopic world. Mesoscopic physics, and the previously mentioned area of nanotechnology in particular, is one of the most active research areas to emerge in modern physics, and the reason for the interest is at least twofold. In addition to exhibiting well-proven technological and commercial potential, the field of mesoscopic physics also motivates research for its novel underlying physics. Mesoscopic devices, such as quantum dots, or "artificial atoms", probe the border between classical physics and purely microscopic, quantum physics, and are expected to play an important role in future electronic appliances.

2.1 Magnetoelectronics and ferromagnetism

The concept of magnetoelectronics was briefly touched upon in Chap. 1, and here we seek to elaborate a bit further on the subject. As mentioned, magnetoelectronics is a field of mesoscopic physics that seeks to use both the charge and the spin of the electron in modern circuitry. For this reason, magnetoelectronics is also often referred to as spintronics, short for "spin transport electronics". The fact that electrons have an internal spin, in addition to a charge, means that functionality and performance of magnetoelectronic devices can be increased compared to their conventional, electronic counterparts.

For magnetoelectronics to be useful, we need efficient ways of producing and detecting currents of spin. Inserting ferromagnetic elements in conductors is one way of achieving this. The internal magnetic moments in ferromagnets are aligned at temperatures lower than the Curie temperature. The ferromagnetic elements cobalt and iron, both widely used in magnetoelectronic devices, have Curie temperatures

exceeding 1000 K, while nickel, another popular ferromagnet, has a Curie temperature of 627 K. A ferromagnet can either have all internal moments aligned in the same direction, in which case it is called a single domain ferromagnet, or it can have internal regions, or domains, where all magnetic moments inside the domain are parallel. At temperatures above the Curie temperature, thermal energy randomises the direction of the magnetic moments, and the material is said to be paramagnetic. To appreciate why certain materials are ferromagnetic below the Curie temperature, one must consider the combined effect of the electron spin and the exclusion principle. Due to the exclusion principle, fermions with parallel spins tend to be separated by a greater distance than fermions with anti-parallel spins. The greater separation reduces the Coulomb repulsion between the charged electrons, and will, for materials such as nickel, cobalt and iron, result in a ferromagnetic ordering of the material. The energy difference between the anti-parallel and the parallel alignment of two spins is called the exchange energy.

The exchange energy shifts electron bands either up or down in energy. Thus, the Fermi level density of states, which determines scattering rates and conductivity, is different for the two spin directions. The spin-dependent asymmetry in conductivities can be used to efficiently produce a net flow of spin angular momentum, as an imbalance in the number of up- and down-spins is observed at the far side of the ferromagnetic element.

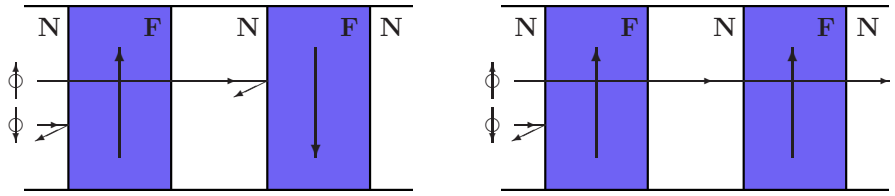

(a) High resistance configuration **(b)** Low resistance configuration

Fig. 2.1: Principles of giant magnetoresistance: The resistance of a conductor with alternating magnetic (F) and non-magnetic (N) elements depends on the magnetic configuration of the heterostructure. In absence of external magnetic fields, a weak anti-ferromagnetic coupling results in the configuration sketched in 2.1(a), characterised by high electrical resistance. Application of an external magnetic field can overcome the coupling and align the magnetisations, as in 2.1(b), resulting in significantly lower resistance.

The applicability and importance of this spin-dependent resistance is clearly displayed in setups exhibiting GMR, short for giant magnetoresistance. The effect, which was discovered in 1988 by independent research teams led by Peter Grünberg [11] and by Albert Fert [12], is most notable for being the basis of read heads in today's hard disk drives. The GMR effect is observed in conductors made up of alternating ferromagnetic and non-magnetic layers, as sketched in Fig. 2.1. Initially, a weak anti-ferromagnetic coupling between the magnetic layers ensures an anti-parallel configuration of the successive magnetisations, as in Fig. 2.1(a). In the figure, we assume that spins parallel to the magnetisation vector experience

low resistance. Thus, the magnetic configuration in Fig. 2.1(a) results in high a resistance, since electrons of both spin directions encounter a ferromagnetic element with anti-parallel magnetisation direction. The anti-ferromagnetic coupling can be overcome by application of an external magnetic field, which aligns the two magnetisations as sketched in Fig. 2.1(b). The new configuration exhibits a significantly lower resistance than the previous configuration, since now a part of the incoming electrons traverses the heterostructure with relative ease. Whether spins parallel or anti-parallel to the magnetisation experience low resistance depends on the Fermi level density of states of the ferromagnetic elements, and the energy band mismatch between the ferromagnetic and the non-magnetic elements [13]. The multilayer setup used by Fert *et al.* measured a resistance reduction as high as 80% [12]. The discovery of GMR is often said to mark the birth of magnetoelectronics, and Fert and Grünberg shared the 2007 Nobel prize in physics for their simultaneous discovery of the effect [14].

A related phenomena, also of utmost importance in magnetoelectronic devices, is the spin-transfer torque [15, 16, 17, 18]. This effect is observed when a polarised spin current passes through a ferromagnet, and the polarisation direction of the current is non-collinear to the magnetisation direction of the ferromagnet. This can be achieved in ferromagnet-non-magnetic heterostructures such as those in Fig. 2.1, but with the two magnetisation directions pointing in different, non-collinear directions. The first ferromagnet produces the spin polarised current. Upon entering the second ferromagnet, spins of the polarised current start to precess around the magnetisation direction of this layer. The momentum of the incoming particles varies, so incoming spins precess with different frequencies. This means that the overall transverse spin component varies rather randomly, with an average approaching zero as the number of incoming particles increases. Thus, the component of the incoming spin current polarised transverse to the magnetisation is apparently lost by the current and absorbed by the magnetisation of the ferromagnet. This transfer of angular momentum translates into a torque on the ferromagnetic magnetisation [19, 20, 21, 22]. As first suggested by Slonczewski [15], the effect, called spin-transfer torque, can be used to excite precession or even reverse the magnetisation in ferromagnets. It can be used as a means to detect spin currents in magnetoelectronic structures as well. This is tangible evidence underlining the fact that electron spin is something that can be manipulated, detected and used to great effect in nanoscale structures.

We argued above that a spin current flowing through a ferromagnet affects the magnetisation of the magnet via the spin-transfer torque. As the next logical step, one could ask whether the reverse effect can be observed as well: Can a precessing magnetisation produce spin currents in neighbouring materials? Indeed, a theory of spin *pumping* describes this very process, in which a precessing magnetisation "pumps" electron spins into adjacent materials [23]. As long as the emitted spins are not all returned to the ferromagnet, the net effect of the precessing magnetisation is an increased loss, or dissipation, of angular momentum in the ferromagnet. The effect is very real, and can be observed as increased linewidths, *i.e.* enhanced damping, in ferromagnetic resonance (FMR) experiments [24].

The interaction between electron spin and ferromagnetic order parameters in mesoscopic heterostructures is a rapidly evolving research field, offering rich physics and significant technological and commercial potential. Given the diversity of the field, the above presentation is nothing but a small *amuse-bouche*; a somewhat more detailed account of the interplay between currents and the ferromagnetic magnetisation relevant to this thesis can be found in Chap. 3.

2.2 Superconductivity

As superconductivity is among the key components of the final manuscript presented in this thesis, a brief summary of this phenomenon feels in order. Superconductivity was first observed by the Dutch physicist Heike Kamerlingh Onnes in 1911 [25, 26, 27]. Kamerlingh Onnes found that mercury (Hg), cooled by liquid helium to the cryogenic temperature of 4,2 K, produced dissipationless electric currents. In the following years, superconductivity was observed at similar temperatures in other simple metals as well, notably aluminium, lead and niobium.

What set superconductors apart from non-superconducting materials, are the properties of perfect conductivity and that of perfect diamagnetism below a critical temperature T_c [28]. Perfect conductivity, *i.e.* current flow in the absence of dissipation or energy loss, implies that the current, or supercurrent, can flow uninterrupted until the "end of time". The second characteristic of superconductors, that of perfect diamagnetism, was discovered by Walther Meissner and Robert Ochsenfeld in 1933, while measuring the magnetic field distribution outside tin and lead samples [29]. The magnetic field outside a superconductor is increased as the temperature of the sample is lowered through T_c. By conservation of total magnetic flux, this implies that the magnetic field is reduced inside the superconducting material. Indeed, apart from in a narrow surface layer, the magnetic field is completely expelled from the superconducting material. The thickness of the surface layer is referred to as the London penetration depth, and the perfect diamagnetism, a phenomenon called the Meissner effect, is an important characteristic of superconductors.

Significant theoretical progress in understanding superconductivity was achieved during the 1950s, primarily in the form of the phenomenological Ginzburg-Landau theory [30] and the microscopic BCS theory [31]. The latter theory, proposed by Bardeen, Cooper and Schrieffer in 1957, is based upon Cooper's observation that electrons experiencing an attractive interaction, couple together in so-called Cooper pairs as long as the temperature is sufficiently low. In many conventional superconductors, the origin of the attractive interaction is the second-order electron-phonon coupling with the crystal lattice. An important characteristic of the Cooper pair energy spectrum, is the existence of an energy gap, meaning that a minimum energy, equal to twice the magnitude of the gap, is required to break up a pair of electrons. At low temperatures, interactions with the crystal lattice do not provide the required energy, implying that Cooper pairs flow through the lattice without experiencing any resistance. This is the origin of the above mentioned supercur-

rent. The size of the gap is reduced, and eventually vanishes, as the temperature of the sample is increased towards its critical temperature T_c. Above T_c, the material ceases to be superconducting.

In conventional superconductors, Cooper pairs have no net magnetic moment, which means that the paired electrons have spin pointing in opposite directions. In ferromagnets, on the other hand, the exchange energy favours a parallel alignment of the electron spins. In other words, in structures consisting of *both* superconducting and ferromagnetic elements, there will be a competition between the two ordering parameters. Although ferromagnetism and superconductivity only rarely coexist in the same material, recent progress in manufacturing techniques allow scientists to study the competing order parameters in nanoscale ferromagnet-superconductor junctions. Such a structure is considered in paper [4], and we provide a more in-depth discussion of ferromagnet-superconductor junctions in Chap. 4.

Chapter 3

Magnetisation dynamics in bulk ferromagnets

The giant magnetoresistance is a famous example of how spin can be used to great effect in modern electronic circuitry, and in the domain of information storage in particular. Spin-sensitive devices are most easily fabricated by introducing ferromagnetic elements in electronic circuitry, such as in magnetoelectronic circuits. Fabrication of superior devices depends upon a thorough understanding of the relevant physical mechanisms - only with this insight is it possible to systematically target implementations that reduce size and power consumption and improve performance. In this chapter, magnetisation dynamics of ferromagnets is discussed, with special emphasis on magnetisation damping and on the interaction between current and magnetisation. A spin polarised current flowing through a ferromagnet, transfers part of its angular momentum to the magnetisation. The result is a torque that can move and change the profile of an inhomogeneous magnetisation. The effectiveness with which the current-induced torque moves an inhomogeneous magnetisation is quantified by a coefficient β. The induced motion is opposed by magnetic damping, which in turn is quantified by the phenomenological damping coefficient α. As we will discuss in this chapter, both coefficients are determined by the same microscopic processes, and the resulting magnetisation dynamics are often highly sensitive to the ratio β/α.

3.1 The Landau-Lifshitz-Gilbert equation

The time-evolution of the unit magnetisation vector $\boldsymbol{m}$ in ferromagnets is usually described by the Landau-Lifshitz equation [32]:

$$\frac{\mathrm{d}\boldsymbol{m}(\boldsymbol{r},t)}{\mathrm{d}t} = -\gamma \boldsymbol{m}(\boldsymbol{r},t) \times \boldsymbol{H}_{\mathrm{eff}}(\boldsymbol{r},t). \tag{3.1}$$

Here, γ is the gyromagnetic ratio and $\boldsymbol{H}_{\mathrm{eff}}$ is called the effective magnetic field. For free electrons, $\gamma = 2\mu_B/\hbar$, where μ_B is the Bohr magneton, while the effective field

is determined from the functional derivative of the free energy $F[\boldsymbol{M}]$ of the system:

$$\boldsymbol{H}_{\text{eff}}(\boldsymbol{r},t) = -\frac{\delta F[\boldsymbol{M}]}{\delta \boldsymbol{M}},$$

where $\boldsymbol{M}$ is the instantaneous magnetisation vector. The effective field is usually a sum of any externally applied magnetic fields, various anisotropy fields related to the particular geometry of the ferromagnet, and possible dipole interactions with neighbouring magnetic materials. The Landau-Lifshitz equation describes precessional motion of $\boldsymbol{m}$ about the effective magnetic field with the Larmor frequency $\omega = \gamma|\boldsymbol{H}_{\text{eff}}|$.

When we write the Landau-Lifshitz equation as in Eq. (3.1), it is assumed that the effective field is determined by the *instantaneous* magnetic configuration of the system. This can be justified if the magnetisation dynamics take place on a very long time-scale, so that microscopic degrees of freedom respond immediately to the time-varying magnetisation. If this is not fulfilled, there is a time lag of the effective field response to the current magnetic configuration. The time lag can be accounted for by augmenting the Landau-Lifshitz equation (3.1) with the dissipative Gilbert damping term [33, 34, 23]:

$$\frac{\mathrm{d}\boldsymbol{m}}{\mathrm{d}t} = -\gamma \boldsymbol{m} \times \boldsymbol{H}_{\text{eff}} + \alpha \boldsymbol{m} \times \frac{\mathrm{d}\boldsymbol{m}}{\mathrm{d}t}. \tag{3.2}$$

In Eq. (3.2), which is commonly referred to as the Landau-Lifshitz-Gilbert (LLG) equation, we have dropped the position and time arguments $(\boldsymbol{r},t)$ for sake of notation, and introduced the positive Gilbert damping parameter α. The Gilbert damping term ensures that the magnetisation vector spirals in towards the energy minimum, determined by $\boldsymbol{H}_{\text{eff}}$.

The LLG equation (3.2) is widely used to describe magnetisation dynamics in bulk ferromagnets and in layered magnetic heterostructures, and it is the basis for modelling magnetisation dynamics in ferromagnetic resonance (FMR) experiments [35, 24, 36]. In such experiments, the ferromagnetic sample is placed in an external dc magnetic field. To excite the magnetisation, a small, time-dependent rf field is applied in the transverse directions, causing the magnetisation to precess about the dc field. The power absorption spectrum is then measured as a function of the magnitude of the dc field. The measured spectrum peaks at a resonance frequency determined by the total effective field $\boldsymbol{H}_{\text{eff}}$, and dissipation affects the peak by reducing peak height, *i.e.* the absorbed power at resonance, and by broadening the shape of the curve. The Gilbert damping coefficient is then extracted by measuring the half-width at half-maximum of the resonance peak, which is, according to the LLG equation, proportional to α [24]. In paper [4], which is discussed in Chap. 4, we consider how a slowly precessing magnetisation affects the observed charge and spin currents in a magnetoelectronic heterostructure. Such precessional motion of the magnetisation can be sustained by *e.g.* a weak, transverse magnetic field, such as that used in the described FMR experiments.

3.2 Gilbert damping

To fully realise the potential of magnetoelectronic devices, a thorough understanding of dissipative processes is of utmost importance. Gilbert damping, parametrised by the coefficient α in the LLG equation (3.2), is a restoring force that brings the magnetisation towards an energy minimum. The damping can help eliminate possibly unwanted thermal fluctuations, and the magnitude of α will determine not only the magnitudes of switching fields and currents, but also the time it takes for the magnetisation to reach its stable fixed point. A proper understanding of Gilbert damping would significantly aid in future tailoring of improved magnetoelectronic structures. Thus, mapping the detailed makeup of the damping coefficient is essential not only from a theoretical point of view, but is arguably even more important from a technological and commercial perspective.

Despite these incentives, a complete microscopic understanding of Gilbert damping is yet to be reached. Even though the first studies date back several decades, the sheer amount of processes contributing to dissipation in bulk ferromagnets delays the emergence of any unified, complete picture. Eddy currents, phonon and magnon scatterings, extrinsic and intrinsic spin-orbit interactions and magnetic impurities are some of the contributions to the damping coefficient measured in FMR experiments [24]. Additionally, the already mentioned spin pumping effect introduces an enhanced damping coefficient as long as the emitted spins are efficiently dissipated outside the ferromagnetic film [23].

Some of the first studies of bulk magnetic dissipation were based on the *s*-*d* model of ferromagnetism [37, 38]. In this model, electrons are classified in one of two categories: Localised *d*-electrons provide the magnetic moment, while itinerant *s*-electrons carry current in the material. The spin densities of the two kind of electrons are coupled via an exchange interaction. Within this model, the exchange interaction gives rise to three-particle processes involving the annihilation (creation) of a spin wave and the creation (annihilation) of an electron-hole pair. The itinerant electron spin is flipped during the magnon scattering process, and angular momentum is dissipated when the outgoing electron undergoes spin-orbit scattering [38]. Thus, dissipation of angular momentum is closely associated to the effective lifetime τ_{sf} of the itinerant electron-hole pair. The quantum mechanical treatment was performed by Heinrich *et al.*, who obtained the Gilbert damping coefficient

$$\alpha_{s-d} = \frac{\eta \hbar^2 \nu_F}{2 s_0 \tau_{\mathrm{sf}}}, \tag{3.3}$$

where ν_F is the Fermi energy density of states, s_0 the equilibrium spin density and $\eta < 1$ is the fraction of total spin carried by the itinerant electrons [38]. Thus, it was found that Gilbert damping scales as resistivity, since τ_{sf} is proportional to momentum scattering time τ in simple normal metals [39]: $\alpha \sim \tau^{-1} \sim \rho$, where ρ is the resistivity of the material.

A more general treatment of the problem of magnetic dissipation followed a few years later, when the concept of a "breathing Fermi surface" was introduced [40, 41].

In the presence of a time-dependent magnetisation, the energy levels and the Fermi surface oscillate and distort according to the instantaneous magnetisation via the spin-orbit interaction. The rotating magnetisation generates empty states below the Fermi surface and filled states above, and the electron population needs to constantly adapt to a changing energy environment. This picture explains the notion of a "breathing Fermi surface". The excitations caused by the rotating magnetisation have a finite lifetime τ, which ensures the existence of a time lag before the electron population is able to readjust to the current energy landscape. From the arguments in Sec. 3.1, this translates into a Gilbert damping coefficient $\alpha \sim \tau \sim \rho^{-1}$, *i.e.* proportional to the conductivity of the material.

Based on the above two scenarios, it seems one can expect either a "conductivity-like" or a "resistivity-like" behaviour on the part of magnetic damping. Indeed, a fusion of these qualitative traits was observed in early experiments, which revealed fascinating non-monotonous temperature dependences in cobalt, nickel and iron [35, 42, 43]. Fig. 3.1, adapted from Ref. [35], displays the qualitative temperature dependence of the Gilbert damping in these materials. In the case of cobalt, the

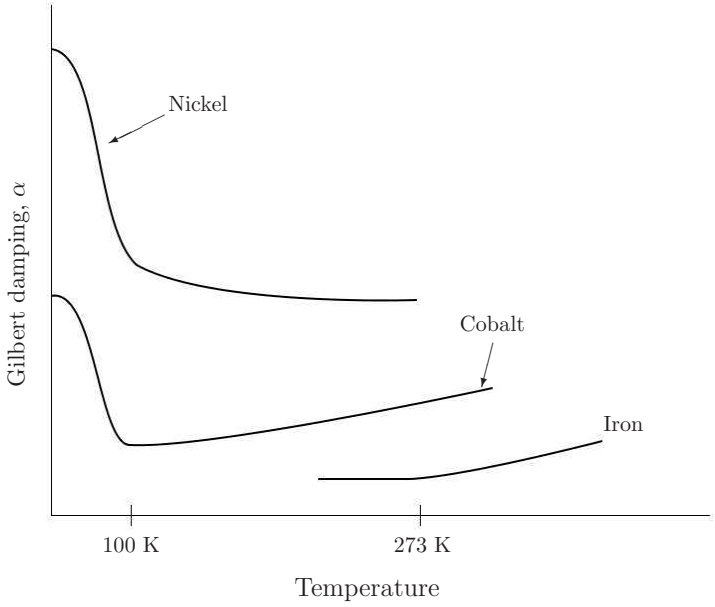

Fig. 3.1: Qualitative temperature dependence of the Gilbert damping in iron, nickel and cobalt. Nickel and cobalt exhibit conductivity-like temperature-dependence below room temperature, while cobalt and iron show resistivity-like behaviour above approx. 100 K and above room temperature, respectively. After Ref. [35].

dissipation initially drops markedly with increasing temperature, before reaching a minimum at approximately 100 K. Nickel exhibits the same sharp drop at low temperatures, before reaching a constant value at room temperature, while iron shows no

temperature dependence below room temperature [35]. Since the initial drop in dissipation observed in cobalt and nickel is reminiscent of the temperature dependence of conductivity, this regime is referred to as the "conductivity-like" contribution to magnetic damping. The linear temperature dependence observed closer to room temperature is the "resistivity-like" contribution. Recently, it has been shown that the torque-correlation model developed by Kamberský [44] describe both these regimes, and fit qualitatively to experimental results at room temperature and below [45]. Better quantitative agreement are yet to be achieved, however, and more studies are required to improve the fundamental understanding of magnetic dissipation and to better guide fabrication of future, superior magnetoelectronic structures.

3.3 Current-induced magnetisation dynamics

As we argued in Sec. 2.1, a spin current flowing through a ferromagnet looses its transverse spin component to the ferromagnetic magnetisation. The transverse component is absorbed as a torque on the local magnetisation, which means that the LLG equation (3.2) needs to be supplemented by a source term whenever a spin current flows through the magnet. In single-domain ferromagnets, transfer of the transverse spin component can be accounted for by including the third term on the right hand side:

$$\frac{\mathrm{d}\boldsymbol{m}}{\mathrm{d}t} = -\gamma \boldsymbol{m} \times \boldsymbol{H}_{\text{eff}} + \alpha \boldsymbol{m} \times \frac{\mathrm{d}\boldsymbol{m}}{\mathrm{d}t} + \frac{\gamma}{M_s V} \boldsymbol{m} \times (\boldsymbol{I}_s \times \boldsymbol{m}), \tag{3.4}$$

where $\boldsymbol{I}_s$ is the spin current and V the volume of the ferromagnet. The spin-transfer term is of the form

$$\boldsymbol{m} \times (\boldsymbol{I}_s \times \boldsymbol{m}) = \boldsymbol{I}_s - \boldsymbol{m}(\boldsymbol{I}_s \cdot \boldsymbol{m}),$$

which equals the transverse spin current component. A source term of this form was initially suggested by Slonczewski [15], and a number of experiments have supported this model for the spin-transfer torque [17, 18, 46, 47, 48, 49]. The LLG equation (3.4) has been frequently applied to various mesoscopic trilayer heterostructures, such as that in Fig. 2.1, where two ferromagnets are separated by a normal metal spacer. The sketched trilayer is usually referred to as a spin valve when it is fabricated so that the magnetisation of the first ferromagnet is pinned by strong anisotropy fields, while the second magnetisation is unpinned. The pinned layer polarise any incoming current, so that the spin-transfer torque can be observed on the second, unpinned magnetisation. The resulting dynamics might yield magnetisation reversal, steady state precessional motion, or a new stable fixed point for the unpinned magnetisation vector, all depending on current amplitude, dissipation and effective magnetic fields.

The situation is more complicated when the magnetisation of the ferromagnet is no longer uniform, but varies in space. When electrons flow through an inhomogeneous magnetisation texture, their spins try to align with the local magnetisation. When the width W of the domain wall is much larger than the typical Fermi wave

vector, *i.e.* $W \gg \lambda_F$, as is the case for most metallic ferromagnets, it is reasonable to assume that the electron spin *adiabatically* aligns with the local magnetisation vector. The equation of motion incorporating the resulting *adiabatic* spin-transfer torque on the magnetic texture is [50, 51, 52]:

$$\frac{\mathrm{d}\boldsymbol{m}}{\mathrm{d}t} = -\gamma \boldsymbol{m} \times \boldsymbol{H}_{\text{eff}} + \alpha \boldsymbol{m} \times \frac{\mathrm{d}\boldsymbol{m}}{\mathrm{d}t} + \frac{\mathscr{P}}{s_0} (\boldsymbol{j} \cdot \boldsymbol{\nabla}) \boldsymbol{m}. \tag{3.5}$$

The quantity $\mathscr{P}$, defined as

$$\mathscr{P} \equiv \frac{\hbar}{2e} \frac{\sigma_\uparrow - \sigma_\downarrow}{\sigma_\uparrow + \sigma_\downarrow},$$

where σ_s is the conductivity for an electron with spin $s\,(=\uparrow,\downarrow)$, is a constant that converts charge current to spin current. The charge current density is denoted by $\boldsymbol{j}$, and s_0 is the equilibrium spin density.

Analytical [52, 53] and numerical [54] studies based on the adiabatic torque in Eq. (3.5) divided the resulting dynamics into two regimes: When the applied electric current is below a certain critical value, the effect of the adiabatic torque is to slightly deform and move the domain wall. The wall motion is quickly decelerated, however, as the injected spin current is dissipated via the anisotropy field of the domain wall. Thus, the adiabatic spin-transfer torque itself does not induce steady wall motion when the applied current is below the critical value. Currents exceeding the critical value on the other hand, generate a time-dependent domain wall velocity whose average value eventually scales linearly with applied current density [53, 54]. The value of the critical current is determined by the detailed anisotropy fields and domain wall width. It was quickly realised, however, that the computed critical current was at least an order of magnitude greater than that observed in experiments [55, 56]. This suggested that the formulation of the spin-transfer process contained in Eq. (3.5) is incomplete.

It is known that spin dephasing processes in ferromagnets contribute to the total dissipation of angular momentum, and thus the Gilbert damping constant α. In a magnetic texture, these processes will also cause mistracking between carrier spins and the local magnetisation texture, and in turn an additional current-induced torque. Thus, spin dephasing processes introduce a new, *non-adiabatic* spin-transfer torque that needs to be accounted for in the magnetic equation of motion. Inclusion of this torque, in the form of the so-called β-term, results in the following LLG equation for the magnetisation vector [57]:

$$\frac{\mathrm{d}\boldsymbol{m}}{\mathrm{d}t} = -\gamma \boldsymbol{m} \times \boldsymbol{H}_{\text{eff}} + \alpha \boldsymbol{m} \times \frac{\mathrm{d}\boldsymbol{m}}{\mathrm{d}t} + \frac{\mathscr{P}}{s_0} (1 - \beta \boldsymbol{m}\times) (\boldsymbol{j} \cdot \boldsymbol{\nabla}) \boldsymbol{m}, \tag{3.6}$$

where β depends on the ferromagnetic exchange interaction and relevant spin dephasing processes. In the present context, *non-adiabaticity* does not refer to an abrupt or rapidly varying domain wall, but rather the angular momentum mismatch introduced by spin dephasing. The coefficient β is often assumed to be of the same order as the Gilbert coefficient $\beta \sim \alpha \ll 1$. In other words, the magnitude of

the non-adiabatic torque is initially much smaller than the adiabatic torque. The β-term does affect magnetisation dynamics qualitatively different than the adiabatic torque, however, and its inclusion in the LLG equation is often essential. As can be seen from Eq. (3.6), the form of the β-term is similar to a magnetic field in the equation of motion, and will, as the magnetic field, determine steady state velocity and shape of a domain wall. To demonstrate this, paper [1] considered a head-to-head Néel wall, where the magnetisation lies in the y-z plane, pointing along the positive z-axis when $z \to -\infty$, and along the negative z-axis for $z \to +\infty$. Assuming that the domain wall can be described by its width, centre position and out-of-plane tilt angle, *i.e.* the widely used Walker ansatz [58], it can be shown that the steady state velocity of the considered Néel wall is given by:

$$v(t \to \infty) = -\frac{\beta}{\alpha}\frac{\mathscr{P}j}{s_0} = \frac{\beta}{\alpha}v(t=0), \tag{3.7}$$

in the absence of magnetic driving fields [57, 59, 1]. In Eq. (3.7), we have substituted for the initial domain wall velocity

$$v(t=0) = -\frac{\mathscr{P}j}{s_0},$$

to emphasise the importance of the ratio β/α on the steady state velocity. This underlines the qualitative difference between the adiabatic and non-adiabatic spin-transfer torques, and shows that the terminal velocity of domain walls is governed by the β-term, for small electric currents. The domain wall motion is sustained by the continuous mistracking of electron spins and the local magnetisation texture.

Analytical progress much beyond the Walker ansatz remains limited, but micromagnetic simulations based on Eq. (3.6) supports analytical predictions and qualitatively confirm experiments on current-induced spin-torques in domain walls [59, 55]. Fig. 3.2, adapted from Ref. [59], shows domain wall velocity as a function of the initial domain wall velocity $-\mathscr{P}j/s_0$, for different values of β/α in a perfect wire. There are no external magnetic driving fields present.

The $\beta = 0$ curve confirms the time-averaged domain wall velocity reported by Tatara and Kohno for the adiabatic torque [53], which is $\sim \sqrt{j^2 - j_{\mathrm{cr}}^2}$, with j_{cr} being the critical current density mentioned above. The average velocity eventually grows linearly with current density, when the applied current far exceeds the critical value. For non-zero β, the numerical results reported in Ref. [59] agree remarkably well with the prediction in Eq. (3.7).

The presented analytical and numerical results suggest that current-induced magnetisation dynamics in domain walls are indeed captured by the LLG equation

$$\frac{\mathrm{d}\boldsymbol{m}}{\mathrm{d}t} = -\gamma \boldsymbol{m} \times \boldsymbol{H}_{\mathrm{eff}} + \alpha \boldsymbol{m} \times \frac{\mathrm{d}\boldsymbol{m}}{\mathrm{d}t} + \frac{\mathscr{P}}{s_0}(1 - \beta \boldsymbol{m}\times)\,(\boldsymbol{j} \cdot \boldsymbol{\nabla})\,\boldsymbol{m}.$$

To improve the quantitative agreement with experimental results, and to better understand the underlying physics, several reports have microscopically investigated

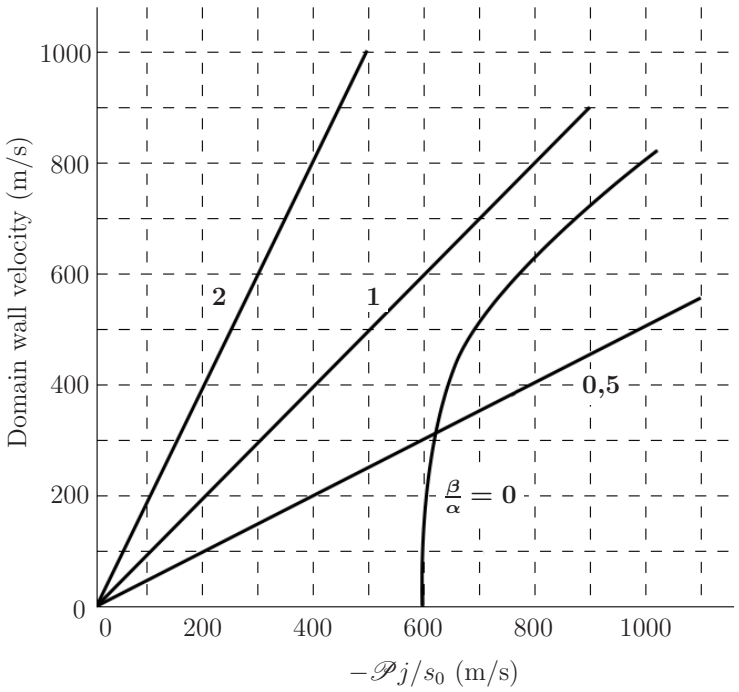

Fig. 3.2: The steady state domain wall velocity of a perfect wire as a function of the adiabatic torque driven velocity $-\mathscr{P}j/s_0$ for different values of β/α with zero magnetic driving field. After Ref. [59].

the α and β coefficients. Even though they both come from band structure and spin dephasing processes, it has become apparent that there are no general symmetry properties relating them, and their values depend on the model and processes considered [1, 9, 10].

3.4 Damping and non-adiabatic torque in itinerant ferromagnets

From the brief survey presented in Secs. 3.2 and 3.3, it is clear that the two dimensionless parameters α and β profoundly affect magnetisation dynamics in ferromagnets. In single-domain ferromagnets for instance, the magnitude of α directly influences the switching time of the magnetisation and the critical current required to achieve such reversal in spin valve structures. In inhomogeneous magnetisation textures such as domain walls, the ratio β/α determines the terminal velocity and the shape of the wall. The focus of this section is research papers [1] and [2], and the main results and insights from our own studies of α and β will be presented.

Much of the reported work on magnetisation damping and current-induced dy-

namics in bulk ferromagnets have used the *s*-*d* model of ferromagnetism as starting point [38, 53, 57]. As mentioned in Sec. 3.2, the *s*-*d* model classifies electrons as belonging to either the localised *d*-orbital or the itinerant *s*-orbital. The two classes of electrons interact via an exchange field that is directed along the magnetic moment of the localised electrons, and current is carried by the itinerant *s*-electrons. An important consequence of this separation is that the localised *d*-electrons are not directly affected by magnetic dissipation due to *e.g.* spin-flip scattering. Loss of angular momentum thus relies on spin dephasing processes involving *s*-electrons only.

There is a strong overlap between *s*- and *d*-orbital electrons in many transition metal ferromagnets, so the applicability of the *s*-*d* model to these materials can be questioned. Papers [1] and [2] consider dissipation and current-induced torque in the alternative Stoner model of ferromagnetism, where current and magnetic moment are carried by the same electrons. Thus, all electrons are prone to spin dephasing in the presence of spin-flip scattering. Much of the calculational details do not depend on the model of ferromagnetism however, so the model-specific results come about when the non-equilibrium spin density is related to the magnetisation, at the end of the calculation [1].

Values for α and β was obtained in paper [1] by explicitly deriving an equation of motion for the non-equilibrium, transverse spin density in the presence of a charge current. The equation for the spin density, which is a quantum Boltzmann equation, can be written in the form of a LLG equation. The two parameters α and β are then readily extracted for the considered model. The microscopic derivation in paper [1] was deliberately limited to weak ferromagnets, *i.e.* ferromagnets where the exchange field is much smaller than the Fermi energy, $\Delta_{xc} \ll E_F$. In this limit, several complex source terms due to scattering, so called collision integrals [60], can be disregarded, and the resulting equation of motion keeps a transparent and rather intuitive form. Additionally, spin relaxation was introduced phenomenologically by an unspecified spin dephasing rate τ_σ^{-1}.

The subsequent paper [2] dealt specifically with the Gilbert damping coefficient, and did not consider the effect of current or an inhomogeneous magnetisation texture on the dynamics. It complimented the previous paper by not assuming weak ferromagnetism and by considering magnetic impurity and extrinsic spin-orbit scattering as specific sources of spin dephasing. The detailed analysis supported the way spin dephasing was phenomenologically included in paper [1]. Additionally, the paper presented specific dephasing rates for the model considered, and it illustrated how the previously ignored corrections to collision integrals affect the microscopic equation of motion. The latter was an essential ingredient to understanding why the results of paper [1] conflicted with related, contemporary studies [9, 10].

In both cases, the starting point for the computations was the single-particle Hamiltonian

$$\mathscr{H} = \mathscr{H}_0 + U(\boldsymbol{r},t) + \frac{1}{2}\big[\Delta_{xc}\boldsymbol{m}(\boldsymbol{r},t) + \gamma\hbar\boldsymbol{H}(\boldsymbol{r},t)\big]\cdot\boldsymbol{\sigma} + \mathscr{H}_\sigma, \tag{3.8}$$

where $\mathscr{H}_0$ is the free particle crystal Hamiltonian and U is the spin-independent

potential, including spin-conserving impurity scattering and, in the case of Ref. [1], a current-generating electric field. The external magnetic field is specified by $\boldsymbol{H}$, $\mathscr{H}_\sigma$ contains any spin dephasing contributions, while $\boldsymbol{\sigma}$ is a vector of the three Pauli matrices. The main quantity of interest in both papers is the spin density $\boldsymbol{s}$, which is related to the density matrix $\rho_{\alpha\beta} = \langle \Psi_\beta^\dagger \Psi_\alpha \rangle$ by the equation

$$\boldsymbol{s}(\boldsymbol{r},t) = \frac{\hbar}{2} \mathrm{Tr}\left\{\boldsymbol{\sigma}\rho\right\}.$$

In the expression for the density matrix, the annihilation (creation) operator for electrons of spin σ is denoted as $\Psi_\sigma^{(\dagger)}$, and the brackets $\langle \cdots \rangle$ indicate thermodynamical averaging. A quantum Boltzmann equation for the non-equilibrium spin density was in both cases derived from a Dyson equation using the Keldysh Green's function technique [60, 61]. The magnetic equation of motion that was obtained in paper [1], identified

$$\alpha = \beta = \frac{\hbar}{\Delta_{xc}\tau_\sigma}, \tag{3.9}$$

for samples with dilute impurity concentrations and a weak exchange field, $\hbar/\tau_\sigma \ll \Delta_{xc} \ll E_F$. Thus, the special point $\beta/\alpha = 1$ is realised in such Stoner models, where the energy bands have a simple, parabolic shape.

The phenomenologically introduced spin dephasing processes give a "resistivity-like", *i.e.* $\sim \tau^{-1}$, contribution to the Gilbert damping coefficient, in agreement with the original *s-d* model study of Heinrich *et al.* [38]. If we assume the Fermi level density of states to be insensitive to the electron spin direction, we can approximate $2s_0 \approx \hbar\Delta_{xc}\nu_F$, where ν_F is the density of states for both spin directions at the Fermi level. Then, the result in Eq. (3.9) can be written

$$\alpha \approx \frac{\hbar^2\nu_F}{2s_0\tau_\sigma} = \frac{\alpha_{s-d}}{\eta}.$$

As in Sec. 3.2, $\eta < 1$ is the ratio of angular momentum carried by *s*-electrons in the *s-d* model, and α_{s-d} is the Gilbert damping from Eq. (3.3). The fact that $\alpha_{s-d} < \alpha$ should not be surprising, since only itinerant electrons undergo spin dephasing in the *s-d* model, while *all* electrons contribute to dissipation in the Stoner model. Recalling the discussion of domain wall motion in Sec. 3.3, and the result in Eq. (3.7) in particular, the special point $\alpha = \beta$ means that the initial and terminal velocities of the considered Néel domain walls are equal. The result $\alpha = \beta$ also suggests that the steady state width W_f of the domain wall is slightly increased compared to the equilibrium value W:

$$W_f = \left(1 + \frac{(\mathscr{P}j)^2\hbar}{2\gamma A\Delta_{xc}s_0^2}\right) W,$$

where A is the exchange stiffness of the domain wall [1].

The complimentary paper [2], devoted to the Gilbert damping parameter, found the same result for α, *i.e.* the result in Eq. (3.9), with spin dephasing rate

$$\frac{1}{\tau_\sigma} = \frac{1}{\tau_{\mathrm{so}}} + \frac{1}{\tau_{\mathrm{m}}},$$

where $\tau_{\rm so}^{-1}$ and $\tau_{\rm m}^{-1}$ are the scattering rates associated with extrinsic spin-orbit and magnetic impurity scattering, respectively. The scattering rates depend on the detailed characteristics of the scattering potential. In paper [2], random, short-ranged potentials were assumed. More specifically, a Gaussian distributed scalar scattering potential with zero average $\langle V(\boldsymbol{r})\rangle = 0$, and white noise correlator $\langle V(\boldsymbol{r})V(\boldsymbol{r}')\rangle = \xi\delta(\boldsymbol{r}-\boldsymbol{r}')$ was considered. Similarly, the magnetic impurity potential was characterised by the white noise correlation amplitudes $\xi_\perp$ and $\xi_{||}$ as in Ref. [9]. The scattering rates were obtained from the quantum Boltzmann equation, and found to be:

$$\frac{1}{\tau_{\rm so}} = \frac{2\pi\Delta_{xc}}{9s_0}\xi\lambda^2\left[(\nu_\uparrow^2 k_{F\uparrow}^4 + \nu_\downarrow^2 k_{F\downarrow}^4) + 2\nu_\uparrow\nu_\downarrow k_{F\uparrow}^2 k_{F\downarrow}^2\right],$$

and

$$\frac{1}{\tau_{\rm m}} = \frac{\pi\Delta_{xc}}{s_0}\left[\xi_\perp(\nu_\uparrow^2+\nu_\downarrow^2) + 2\xi_{||}\nu_\uparrow\nu_\downarrow\right].$$

In these equations, ν_σ and $k_{F\sigma}$ are the Fermi level density of states and momentum for spin-σ electrons, respectively, while the amplitude of the spin-orbit coupling is given by the parameter $\lambda = -\hbar^2/4m_e^2c^2$.

Before concluding this section, some comments about the assumption of weak ferromagnetism in paper [1] are in order. Shortly after paper [1] was made available online, a calculation of α and β that was not restricted to weak ferromagnets was reported by Kohno *et al.* [9]. The report, which presented an elegant diagrammatic imaginary time calculation, found that $\alpha \neq \beta$, in general, contradicting the result obtained in [1]. Even though the ratio β/α predicted by the improved treatment *is* close to unity for most transition metal ferromagnets, the result underlined that there are no fundamental symmetries suggesting that the two coefficients are equal in magnitude. On the contrary, involved impurity potential anisotropies and realistic band structures are expected to contribute differently to α and β. Our follow-up paper was not restricted to weak ferromagnetism, and here we obtained a Gilbert damping coefficient identical to that of the superior imaginary-time formalism of Ref. [9]. We did not obtain an expression for β, however, due to technically involved calculations. Results confirming those of Kohno *et al.* was later obtained using an impressive functional Keldysh theory formulation [10].

3.5 Current-driven domain wall dynamics in ferromagnetic semiconductors

As we have seen, spin dephasing processes determine both the Gilbert damping coefficient α and the non-adiabatic torque parameter β. Processes involving dissipation of angular momentum contribute to α, and the same mechanisms introduce a mismatch between carrier spins and the local magnetisation texture, even in the limit of a very wide domain wall. In addition to the discussed spin-flip scattering, complicated band structures is another possible source of spin mistracking, and, in turn, a non-adiabatic torque. Ferromagnetic semiconductors, which exhibit strong intrinsic

spin-orbit interaction, is an example of a system in which such band structure effects are expected to play a key role. Experimental evidence suggest that the current den-

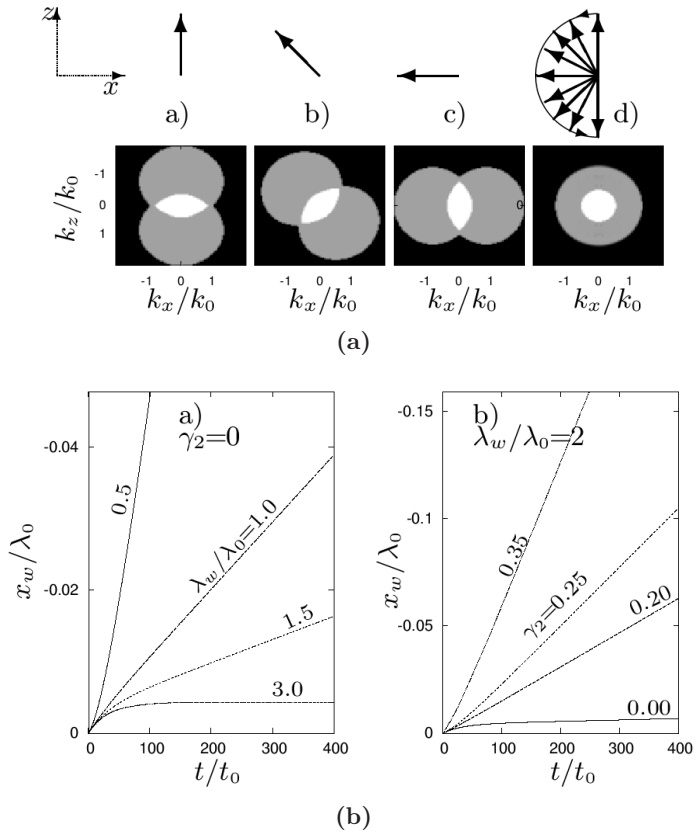

Fig. 3.3: The dependence of transverse propagating modes on the magnetisation vector in (Ga,Mn)As is illustrated in 3.3(a). The top arrows indicate local magnetisation direction, while the white (grey) cross-section correspond to two (one) propagating spin channels. In 3.3(b) the calculated domain wall displacement for zero spin-orbit coupling (left), and varying spin-orbit coupling strength γ_2 (right) is shown. Further details can be found by consulting paper [3].

sity needed to move a domain wall in ferromagnetic semiconductors is two to three orders of magnitude lower than in ferromagnetic metals [62, 63]. This observation make ferromagnetic semiconductors highly interesting for *e.g.* magnetic random access memory devices. The purpose of paper [3] was to illustrate numerically how the intrinsic spin-orbit coupling in the ferromagnetic semiconductor (Ga,Mn)As enhances the non-adiabatic torque and the domain wall velocity, compared to systems with simple parabolic energy bands.

In itinerant, bulk ferromagnets with simple parabolic bands, carrier spins are

assumed to align themselves adiabatically to the local, slowly varying magnetisation texture. In clean ferromagnets, the intrinsic domain wall resistance vanishes in the adiabatic limit, where domain wall width far exceeds the Fermi wavelength. This is no longer true for systems exhibiting intrinsic spin-orbit coupling, since now the carrier wave vector and spin are coupled by the spin-orbit interaction. The anisotropy introduced in the distribution of propagating modes as the carrier spin adiabatically aligns with the local magnetisation texture, leads to carrier reflection and increased domain wall resistance [64]. The anisotropy in mode space is illustrated in Fig. 3.3(a), where the effect is shown for a spin traversing a Bloch wall. Only modes with transverse wave vectors lying inside the circular cross-sections shown to the far right in Fig. 3.3(a) contribute to the overall conductivity. Modes outside this area are eventually blocked, leading to finite resistance in the structure [64], and mistracking between carrier spins and the local magnetisation [3].

The effect of intrinsic spin-orbit coupling on domain wall displacement is shown in Fig. 3.3(b), where the left-most graph corresponds to vanishing spin-orbit coupling, $\gamma_2 = 0$, and varying domain wall width. As expected, the terminal domain wall velocity approaches zero as the width λ_w exceeds the Fermi wave length λ_0, and deviations from perfect adiabaticity are reduced. The right-most graph in Fig. 3.3(b) shows the effect of intrinsic spin-orbit coupling on the non-adiabatic torque and the domain wall terminal velocity. The numerical study in paper [3] found a substantial three to four order increase in domain wall velocity when a ferromagnetic metal is replaced by a (Ga,Mn)As sample. These findings offer ample evidence of how a β-term is produced in clean systems, by a non-trivial band structure. Finally, the fact that the simulations were performed in clean systems might explain why the calculated increase in domain wall velocity is larger than the experimentally observed two to three order increase [62, 63].

Chapter 4

Pumped currents in a ferromagnet-superconductor junction

To no degree can the previous chapter do justice to the rich physics or the wealth of intriguing phenomena caused by the interaction between current and the magnetic order parameter. This is arguably one of the most exciting fields of contemporary magnetoelectronics, not least because of its significant technological and commercial potential. The focus of Chap. 3 was bulk ferromagnets and the effect of polarised spin currents on the macroscopic magnetisation. As we have pointed out, however, the opposite effect can also be observed: While a spin polarised current generates magnetisation dynamics, an excited magnetisation can pump angular momentum into adjacent materials and produce spin currents. Spin pumping by a precessing magnetisation is a key ingredient in the present chapter and in paper [4], where we study how magnetisation motion and superconducting correlations affect charge and spin currents in a normal metal-ferromagnet-superconductor junction. Before the main findings of paper [4] are communicated, we briefly review the important Andreev reflection process and some recent developments in the field of proximity effects.

4.1 Andreev reflection

As mentioned in Sec. 2.2, the energy spectrum of a superconductor is characterised by a finite gap at low temperatures. Still, the conductance of a normal metal-superconductor junction is finite; indeed, it is twice that of a normal metal-normal metal junction when the normal metal is in good contact with the superconductor. The question that naturally arises then, is how charge is transferred between a non-superconducting material and a superconductor, when the carrier energies lie well inside the superconducting gap?

The solution to this apparent conundrum is a process called Andreev reflection,

after Russian physicist Alexander F. Andreev [65]. To illustrate the process, we consider an electron with charge e just above the Fermi energy, approaching a normal metal-superconductor interface from the normal side. There are no available states at this energy in the superconductor, so the electron couples together with another electron situated just below the Fermi energy, and enters the superconductor together with the coupled electron as a Cooper pair. Thus, for every Andreev reflection, a total charge $2e$ is transferred to the superconductor since the process involves transmission of two electrons. The second transmitted electron leaves behind a hole that is reflected away from the normal metal-superconductor interface [65, 66]. Using the popular Blonder-Tinkham-Klapwijk framework, one readily observes that the conductance of a perfect normal metal-superconductor junction is twice that of a normal metal-normal metal junction, *i.e.* $G_{NS} = 2G_{NN}$ [67].

Andreev reflection is compared to normal reflection in Fig. 4.1. Normal scattering, the process that takes place at *e.g.* a normal metal-insulator interface, is depicted in Fig. 4.1(a). Since no charge is transferred to the insulating side, charge is conserved during the process. The total momentum, however, is in general not conserved. The opposite is seen when the insulator is replaced by a superconductor: Now total charge $2e$ is transferred to the superconducting side, while the total momentum is (approximately) conserved.

(a) Normal reflection **(b)** Andreev reflection

Fig. 4.1: Andreev reflection process: 4.1(a) Normal reflection at a normal metal-insulator interface, where no net charge is transferred across the interface. 4.1(b) The insulator is substituted with a superconductor, and charge $2e$ is transferred into the superconductor by means of Andreev reflection.

In conventional superconductors, Cooper pairs are made up of electrons with opposite spins. Thus, as a spin-up electron in the normal metal approaches the superconductor, it pairs with a spin-down electron upon transmission. This means that the reflected hole on the normal side has opposite spin compared to the incoming electron. As will be further explored in the next section, spin sensitivity of Andreev reflection processes leads to rich and unexpected phenomena in these mesoscopic heterostructures.

4.2 Proximity effects in mesoscopic heterostructures

The BCS theory that was briefly outlined in Sec. 2.2, is the prevalent theory of superconductivity, and explains how a weak, phonon-mediated attraction between electrons results in Cooper pairs that flow unhindered through the crystal lattice at low temperatures. Properties of these superconducting correlations are now studied extensively, largely aided by an ever-increasing level of technological sophistication by which new mesoscopic heterostructures are fabricated [68, 69]. It is now possible to make high-quality normal metal-superconductor junctions, where the length of the normal metal is of the same order as the superconducting coherence length. This implies that one can perform detailed measurements of how the superconductor affects physical properties of the normal metal.

When a superconductor is in good contact with a non-superconducting material, Cooper pairs penetrate into the non-superconducting side of the junction. The introduction of finite superconducting correlations in a non-superconducting material is known as the proximity effect [70]. Andreev reflection, which was the topic of Sec. 4.1, and one of the key processes studied in paper [4], is an important example of the proximity effect. The reflected hole will (almost) retrace the path of the incoming electron, but also obtain a phase relative to the incoming electron. The obtained phase is given by the phase of the superconductor and the ratio of the particle energy to the magnitude of the superconducting gap. In a clean normal metal at temperature T, the electron-hole correlations persist over a length given by the thermal coherence length of the metal, $\xi_{N,0} = \hbar v_F / k_B T$. In the diffusive regime, the coherence length is determined by the diffusion coefficient D_N of the normal metal, $\xi_N = \sqrt{\hbar D_N / k_B T}$. Thus, especially at low temperatures, superconducting correlations exist far into the normal metal region and, as the size of fabricated heterostructures gradually become smaller, might even extend throughout the entire normal metal. The presence of superconducting correlations on the normal side leads to a small gap in the energy spectrum and a suppression of the normal density of states [71].

Another example of the proximity effect and long-range superconducting correlations, is the famous Josephson effect [72, 73]. When two bulk superconductors are connected by a weak link, *e.g.* a tunneling barrier or a normal metal that is made weakly superconductive due to the proximity effect, a zero voltage supercurrent flows through the structure as long as there is a finite phase difference between the superconductors. Brian D. Josephson predicted a simple sine-dependence of the supercurrent on the phase difference, and this is known as the dc Josephson effect in superconductor-weak link junctions. The ac Josephson effect is observed when a finite voltage bias is applied across the weak link: In this case the phase difference becomes time-dependent, resulting in an alternating current with frequency $2eV/h$, where V is the applied voltage and h is Planck's constant [72]. Josephson was awarded one half of the Nobel Prize in Physics in 1973 for his theory on the

Josephson effect [74].

The leakage of Cooper pairs into a normal metal will not only affect physical properties of the receiving material, but also the superconductor itself. Thus, in addition to the above mentioned proximity effects, there are also *inverse* proximity effects. An example of the inverse effect in normal metal-superconductor junctions, is the reduction of the superconducting order parameter close to the junction on the superconductor side. Reduced superconductivity manifests itself in a lowered critical temperature of the condensate, a temperature that is reduced as the length of the non-superconducting region is increased [70].

So far, we have not discussed proximity effects in structures where there is a definite spin ordering on the non-superconducting side of the junction. As pointed out above, Cooper pairs in conventional superconductors do not have any net magnetic moment attached to them, *i.e.* the pairs are composed of electrons with opposite spins. In a ferromagnet, the exchange field lifts spin degeneracy and make a certain spin direction more energetically favourable than the other. This ordering is rather incompatible with singlet Cooper pairs, as the exchange interaction breaks up pairs of opposite spins. Thus, apart from the exotic, recently discovered ferromagnetic superconductors UGe_2 [75], $ZrZn_2$ [76] and URhGe [77], a layered ferromagnet-superconductor structure is arguably the most promising system for studying interplay between the two competing order parameters.

A number of spin-related effects manifest themselves when a ferromagnet is inserted as the non-superconducting material in these mesoscopic junctions. At the end of Sec. 4.1, it was pointed out that Andreev reflected particles have their spin direction reversed with respect to the incoming particle. This is a consequence of the required singlet nature of Cooper pairs in conventional superconductors. Thus, in a ferromagnet where there are different numbers of transport channels for majority ($n_\uparrow$) and minority spin channels ($n_\downarrow$), only a fraction $n_\downarrow/n_\uparrow$ of the majority spin channels can undergo Andreev reflection. As a result, the conductance of ferromagnet-superconductor junctions is reduced when the ferromagnet has a high degree of spin polarisation. Indeed, the conductance becomes even smaller than that of a ferromagnet-normal metal junction when $n_\downarrow/n_\uparrow < 1/3$, as shown in Ref. [78].

Equally important is the effect of the exchange field on the momentum of the Andreev reflected particle. Depending on spin direction, the momentum is either increased or decreased with respect to the momentum of the incoming particle. The wave vector mismatch, which is significant for common transition metal ferromagnets, results in rapidly decaying superconducting correlations in the ferromagnet. In the diffusive regime, the length scale for the correlation decay is given by $\xi_F = \sqrt{\hbar D_F/\Delta_{xc}}$, where D_F is the diffusion coefficient of the ferromagnet [69]. Thus, the decay length is determined by the exchange field Δ_{xc}, and not the thermal energy k_BT, as in diffusive normal metals. In iron or nickel, ξ_F is of the order of Ångströms, which is much shorter than the penetration length ξ_N associated with normal metal-superconductor junctions, which can reach several hundred nanometres.

More intriguing perhaps, is the observation that superconducting correlations, in

addition to being exponentially decaying, are accompanied by oscillations in space. Thus, the correlation function changes sign at selected points in space as it traverses the uniform ferromagnet, leading to an *increase* in the density of states in certain space intervals [79, 80]. This is contrary to the density of states suppression observed in normal metal-superconductor junctions. Related to the correlation function oscillations is also the emergence of the π-junction [81, 82]. For a Josephson junction in the π-state, the Josephson coupling energy sees a minimum when the phase difference between the superconductors is π. This implies that the Josephson current in a π-state junction flows in the opposite direction to that of an ordinary 0-state junction. Evidence of a π-junction can be seen as the length of the ferromagnet is varied: The critical Josephson current is first reduced, before it switches direction. The effect was predicted several years ago [83, 84], but only recently observed in experiments [80, 85].

Another proximity effect in ferromagnet-superconductor junctions that has received a great deal of attention, is one that was first observed in experiments in the mid- to late-1990s. A most unexpected decrease in resistance of ferromagnet-superconductor junctions was seen as the temperature was lowered through the superconducting critical temperature T_c [86, 87, 88]. The measured resistance drop, which is assumed to take place in the ferromagnetic part of the junction, was found to be twice as large as that predicted by the then-prevalent theory [88]. The experimental results spawned significant theoretical work, which eventually suggested that the resistance drop was indeed due to long-ranged superconducting correlations in the ferromagnet, and that these correlations are insensitive to the pair-breaking exchange field.

The dominating explanation for the observed long-ranged proximity effect in ferromagnet-superconductor junctions, is based on the generation of *triplet* superconducting correlations in the ferromagnet. Contrary to the anti-parallel spin ordering in singlet pairs, parallel spin ordering is possible in triplet Cooper pairs. When two paired electrons have their spins in the direction of the exchange field, they no longer experience the pair-breaking effect of the field, and the corresponding coherence length becomes comparable to that of singlet Cooper pairs in normal metals. Theoretical reports showed that a ferromagnet with an inhomogeneous magnetisation texture would indeed produce triplet correlations with amplitude comparable to the short-ranged singlet correlations [89, 90], and that the resulting resistance drop at T_c could be comparable to that of normal metal-superconductor junctions. It is now established that a inhomogeneous magnetisation texture, such as a domain wall, various spin-flip sources and even a precessing, single-domain magnetisation vector can produce long-ranged correlations in a ferromagnet [91, 92]. However, it remains to be verified whether inhomogeneous magnetic regions are actually present in the heterostructures used in experiments. Recommended in-depth reviews of proximity effects in ferromagnet-superconductor junctions and long-ranged triplet correlations can be found in *e.g.* Refs. [69, 91].

Inspired by the exotic and rich proximity physics discussed above, and insights from spin pumping theory [23], paper [4] details a theoretical investigation of charge

and spin currents in a ferromagnet-superconductor junction. Motivated in part by the model study recently reported by Houzet [92], we considered how the process of Andreev reflection contributes to charge and spin currents pumped by a precessing, spatially uniform magnetisation vector. The theoretical framework and main results from the paper are described in the following sections.

4.3 Scattering formulation

The spin pumping theory, which describes how a time-dependent magnetisation vector affects charge and spin currents in spin valves and similar structures, dates back several years. It is well known that in the absence of voltage bias, a precessing magnetisation pumps a pure spin current, with no accompanying charge flow. The pumped spin current has vector components along $\partial_t \boldsymbol{m}$ and $\boldsymbol{m} \times \partial_t \boldsymbol{m}$. Both directions are transverse to the magnetisation unit vector $\boldsymbol{m}$, with respective magnitudes given by the imaginary and real part of the mixing conductance [23]. The latter is a complex-valued conductance parameter defined as the off-diagonal spin components of the conductance matrix:

$$g_{N|F}^{\uparrow\downarrow} \equiv \sum_{m,n} \left[\delta_{m,n} - r_{mn}^{\uparrow} (r_{mn}^{\downarrow})^* \right], \tag{4.1}$$

where (m,n) denote transport channels and r^σ is the reflection amplitude for a spin-σ carrier impinging on the ferromagnet interface from the normal metal side.

To study how Andreev reflections affect the familiar results from normal metal-ferromagnet junctions, we study the model sketched in Fig. 4.2. At either end, we

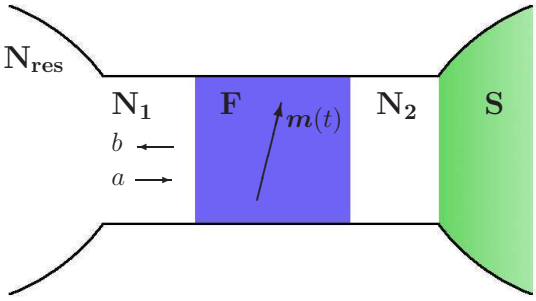

Fig. 4.2: Sketch of the normal metal-ferromagnet-superconductor trilayer studied in paper [4]. The normal metal reservoir $\mathrm{N_{res}}$ is connected to a superconductor S via the ferromagnetic scattering region F. Right-going charge and spin currents are calculated in ballistic lead $\mathrm{N_1}$ in response to a precessing magnetisation $\boldsymbol{m}(t)$ in F, and a bias voltage V applied to the normal side of the structure.

place particle reservoirs that are assumed to be in thermal equilibrium. The normal metal reservoir $\mathrm{N_{res}}$ at the left hand side, is connected to a ferromagnetic scattering region via a ballistic normal lead $\mathrm{N_1}$. We assume that any bias voltage V is

applied at the normal metal side of the structure. Similarly, the superconducting reservoir S is coupled to the scattering region via ballistic normal lead N_2. We take couplings between reservoirs and leads to be ideal, which means that only Andreev reflection takes place at the $N_2|S$ interface, and that all left-moving carriers in N_1 exit reflectionless into N_{res}. The insertion of ballistic lead N_2 is a conceptual simplification that spatially separates the two scattering processes that we study, *i.e.* spin-dependent scattering in the ferromagnet, and Andreev reflection at the superconductor interface, and allows us to describe transport by well-defined scattering states in the two leads. The magnetisation is uniform throughout the ferromagnetic scattering region, and the exchange field Δ_{xc} is of constant magnitude along $\boldsymbol{m}(t) = (\sin\theta(t)\cos\Omega t, \sin\theta(t)\sin\Omega t, \cos\theta(t))$. Here, $\theta(t)$ is the time-dependent polar angle of the magnetisation, while Ω is the precessional frequency about the z-axis. The motion of $\boldsymbol{m}$ can be sustained by *e.g.* a weak, external FMR field, as suggested in Sec. 3.1. In paper [4], $\boldsymbol{m}$ is the sole pumping parameter.

A mean field BCS Hamiltonian is assumed applicable for the superconducting reservoir:

$$\mathscr{H} = \sum_{\sigma=\uparrow,\downarrow} \int \mathrm{d}\boldsymbol{r}\; \psi_\sigma^\dagger(\boldsymbol{r}) \mathscr{H}_0(\boldsymbol{r}) \psi_\sigma(\boldsymbol{r}) + \int \mathrm{d}\boldsymbol{r}\; \left\{ \Delta(\boldsymbol{r}) \psi_\uparrow^\dagger(\boldsymbol{r}) \psi_\downarrow^\dagger(\boldsymbol{r}) + \Delta^*(\boldsymbol{r}) \psi_\downarrow(\boldsymbol{r}) \psi_\uparrow(\boldsymbol{r}) \right\},$$

where $\mathscr{H}_0$ is the normal state, single-particle Hamiltonian and $\Delta(\boldsymbol{r})$ is the superconducting gap. We apply the "rigid boundary condition" described in Ref. [66], and model the gap by a step function at the $N_2|S$ interface: $\Delta(\boldsymbol{r}) = \Delta \mathrm{e}^{\mathrm{i}\phi}\Theta(x)$, where x is the coordinate perpendicular to this interface, and ϕ is the constant phase of the superconductor. This approximation for the superconducting order parameter disregards the *inverse* proximity effect discussed in the previous section, but superconducting correlations induced on the normal side of the interface are fully included, however.

In the following, we limit our attention to particle energies below the superconducting gap, or, to be more specific, we consider the situation where $eV \leq \Delta \ll \Delta_{xc}, E_F$. In this energy regime there is no ordinary transmission through the $N_2|S$ interface. This means that any left-moving particle in lead N_1, *i.e.* an "outgoing" particle, can be related to a set of right-moving particles, or "incoming" particles, in the same lead. Letting b_α (a_β) be the second-quantised operator that annihilates outgoing (incoming) scattering state α (β), we relate the operators as follows:

$$b_\alpha(t) = \sum_\beta \int \mathrm{d}t'\; \mathcal{S}_{\alpha\beta}(t,t') a_\beta(t'), \tag{4.2}$$

where $\mathcal{S}$ is the scattering matrix for the system, and the indices (α,β) completely determine the scattering state in question, *i.e.* both spin, transport mode and whether the state is electron- or hole-like. Due to the assumption that any left-moving carriers in N_1 exit without reflection into the normal reservoir, there is no mixing between right- and left-moving carriers in this lead. Thus, all right-moving carriers in N_1 follow the known thermal distribution function of the normal reservoir.

Once we determine the makeup of the scattering matrix $\mathcal{S}$, we can derive currents from the generalized current operator [93]

$$I_{\alpha\beta}(t) \equiv 2\pi\tau^z_{\alpha\alpha}\left(a^\dagger_\alpha(t)a_\beta(t) - b^\dagger_\alpha(t)b_\beta(t)\right),$$

where τ^z is a diagonal matrix in electron-hole space:

$$\tau^z = \begin{pmatrix} 1 & 0 \\ 0 & -1 \end{pmatrix}.$$

From this operator, the right-flowing charge and spin currents in N_1 are obtained from the prescriptions

$$I_c(t) = \sum_\alpha \langle I_{\alpha\alpha}(t)\rangle, \tag{4.3}$$

and

$$\boldsymbol{I}_s(t) = \frac{\hbar}{2e}\sum_{\alpha,\beta}\boldsymbol{\rho}_{\alpha\beta}\langle I_{\beta\alpha}(t)\rangle, \tag{4.4}$$

respectively. The angular brackets $\langle\cdots\rangle$ imply thermal averaging, and $\boldsymbol{\rho}$ is a matrix with the electron-hole space structure

$$\boldsymbol{\rho}_{\alpha\beta} = \begin{pmatrix} \boldsymbol{\sigma}_{\alpha\beta} & 0 \\ 0 & \boldsymbol{\sigma}^*_{\alpha\beta} \end{pmatrix},$$

and $\boldsymbol{\sigma}^{(*)}$ is the vector of (complex conjugated) Pauli matrices.

The above formulation of transport theory, which is applied in paper [4], is referred to as scattering theory [94]. In the general time-dependent formulation of Eq. (4.2), this framework captures both ballistic and diffusive transport properties, and is capable of describing systems exhibiting arbitrary time-dependence.

Another framework frequently used in transport studies of superconductor heterostructures is that of quasiclassical Green's functions [60]. This framework has been developed to an extraordinary level of sophistication, and has been applied with great success in describing various non-equilibrium phenomena in normal metal-superconductor heterostructures [95]. Unlike the general scattering theory, however, the quasiclassical formalism is restricted to diffusive transport and to weak ferromagnetism, $\Delta_{xc} \ll E_F$. Thus, quasiclassics is not immediately applicable to strong, transition metal ferromagnets, such as iron, nickel or cobalt, and should only be expected to produce qualitatively correct results for such structures.

In the subgap energy regime, spin-dependent scattering in the ferromagnet and Andreev reflections at the N_2|S interface contribute to the total scattering matrix of the structure. In other words, the total scattering matrix $\mathcal{S}$ is a concatenation of the ferromagnetic scattering matrix s_F and the Andreev reflection matrix r^A. The ferromagnetic scattering region does not convert electron-like carriers to hole-like carriers, or vice versa, so s_F is diagonal in electron-hole space. It has the following structure in lead space:

$$s_F = \begin{pmatrix} r_{11} & t_{12} \\ t_{21} & r_{22} \end{pmatrix}.$$

The matrix components r_{ii} and t_{ij} describe reflection of an incoming electron in mode i, and transmission of an electron from lead j to lead i, respectively. Both r_{ii} and t_{ij} are matrices in spin and mode space. Andreev reflection is described by r^A with the following electron-hole structure:

$$r^A = \begin{pmatrix} 0 & r^A_{eh} \\ r^A_{he} & 0 \end{pmatrix} = \begin{pmatrix} 0 & \mathrm{i}\alpha\sigma^y \mathrm{e}^{\mathrm{i}\phi} \\ -\mathrm{i}\alpha\sigma^y \mathrm{e}^{-\mathrm{i}\phi} & 0, \end{pmatrix}$$

where $\alpha = \exp[-\mathrm{i}\arccos(\varepsilon/\Delta)]$, and ε is the excitation energy, measured with respect to the Fermi level. The above scattering elements are all obtained by demanding continuity of scattering wave functions and their spatial derivatives [66].

When the magnetisation vector in the ferromagnetic region is *static*, the total scattering matrix is simply the spin-generalisation of the well-known normal metal-superconductor scattering matrix, derived in *e.g.* Ref. [66]. The components describing how an incoming electron is reflected as an electron, S_0^{ee}, or as a hole, S_0^{he}, read:

$$\begin{aligned} S_0^{ee}(\varepsilon) &= r_{11}(\varepsilon) + t_{12}(\varepsilon) r^A_{eh}(\varepsilon) r^*_{22}(-\varepsilon) M_e(\varepsilon) r^A_{he}(\varepsilon) t_{21}(\varepsilon), \\ S_0^{he}(\varepsilon) &= t^*_{12}(-\varepsilon) M_e(\varepsilon) r^A_{he}(\varepsilon) t_{21}(\varepsilon), \end{aligned}$$

where $M_e(\varepsilon) = \left[1 - r^A_{he}(\varepsilon) r_{22}(\varepsilon) r^A_{eh}(\varepsilon) r^*_{22}(-\varepsilon)\right]^{-1}$ represents multiple reflections at the F|N_2 and N_2|S interfaces.

Even though the matrices S_0^{ee} and S_0^{he} look involved, they can be understood by simple pictures of the actual scattering processes. For an incoming electron to be reflected as an electron (a hole), it must undergo an even (odd) number of Andreev reflections. Thus, S_0^{ee} is a sum of direct reflection at the N_1|F interface (r_{11}) and a trajectory that sees the electron transmit through the ferromagnet once (t_{21}), undergo an even number of Andreev reflections ($r^A_{eh} r^*_{22} M_e r^A_{he}$), before transmitting back through F (t_{12}). Since scattering in F itself will not turn an electron into a hole, S_0^{he} is made up of transmission through F (t_{21}), an odd number of Andreev reflections ($M_e r^A_{he}$), followed by transmission through F as a hole (t^*_{12}).

The caveat so far is that the above scattering matrices are only applicable for time-independent scattering. Once the magnetisation vector starts precessing, the scattering matrix s_F attains a time-dependence. Simple matrix multiplication is now replaced by time convolutions, which greatly complicates evaluation of the matrices. However, restricting our attention to a slowly oscillating magnetisation vector, we can systematically account for the time-dependence by expanding scattering matrices in the frequencies Ω and $\partial_t\theta$.

It should be pointed out that Moskalets and Büttiker have previously developed a general time-dependent scattering theory in a series of papers, see *e.g.* Refs. [96, 97]. They base their studies on the Floquet matrix $\mathcal{S}(\varepsilon, \varepsilon')$, which is an energy representation of the total scattering matrix, and develop a framework for calculating currents in multiterminal structures. Time-dependent scattering is incorporated by expanding in sideband contributions $\mathcal{S}(\varepsilon, \varepsilon \pm n\hbar\Omega)$ of the scattering matrix, similarly to the way we expand the scattering matrix in magnetisation vector frequency,

mentioned above. The Floquet formulation and the time-dependent formulation are equivalent, and observations made during the work with paper [4] agree with those previously reported by Moskalets and Büttiker.

4.4 Charge and spin currents pumped by a time-dependent magnetisation

Once the scattering matrices $\mathcal{S}^{ee}$ and $\mathcal{S}^{he}$ are determined to first order in frequency of the magnetisation vector, pumped charge and spin currents can be obtained by evaluating Eq. (4.3) and (4.4). As mentioned in Sec. 4.3, only a transverse spin current is pumped by a precessing magnetisation in normal metal-ferromagnet junctions that are in electrochemical equilibrium [23]. A recent study of pumped charge and spin currents in normal metal-ferromagnetic superconductor junctions reported similar qualitative behaviour, but with the mixing conductance (4.1) augmented by Andreev reflection processes:

$$g^{\uparrow\downarrow}_{N|FS} = \sum_{m,n} \left[\delta_{m,n} - r^{\uparrow}_{mn}(r^{\downarrow}_{mn})^* + r^{\uparrow}_{he,mn}(r^{\downarrow}_{he,mn})^* \right]. \tag{4.5}$$

Here r^{σ}_{he} is the electron-hole reflection amplitude for an incoming spin-σ electron [98]. Based on these findings, we expect similar qualitative behaviour for the normal metal-ferromagnet-superconductor structure sketched in Fig. 4.2.

Most of the previous work on spin pumping have been restricted to first-order pumping in structures that are held in electro-chemical equilibrium. In paper [4], we attempt to expand upon previous work by considering the effect of pumping when a finite bias voltage is applied across the structure. As previously reported by Moskalets and Büttiker, time-dependent scattering introduces non-trivial corrections to currents when reservoirs are held at different chemical potentials [96]. These corrections include gradient corrections to the adiabatic scattering matrix that must be calculated explicitly for the specific system at hand. In paper [4], we find that the charge current is not affected by these complications, but that spin current is.

The charge current retains its simple stationary value, and is thus unaffected by the pumping parameter also in normal metal-ferromagnet-superconductor trilayers. The result

$$I_c = \frac{e}{2\pi\hbar} \int_{-\infty}^{\infty} \mathrm{d}\varepsilon \; [f_e(\varepsilon) - f_h(\varepsilon)]\, \tilde{g}(\varepsilon), \tag{4.6}$$

echoes the current derived by de Jong and Beenakker for ferromagnet-superconductor junctions [78], and by Brataas and Tserkovnyak for normal metal-ferromagnetic superconductor junctions [98]. The distribution functions are those of the normal metal reservoir:

$$f_{e(h)}(\varepsilon) = f_0(\varepsilon + (-)eV) = [1 + \exp\{(\varepsilon + (-)eV)/k_BT\}]^{-1},$$

and the total conductance is defined as in Refs. [78, 98]:

$$\tilde{g} \equiv \sum_{m,n} \left\{ \left| \underline{S}^{he}_{\downarrow\uparrow,mn} \right|^2 + \left| \underline{S}^{he}_{\uparrow\downarrow,mn} \right|^2 \right\},$$

where the summation runs over all transport modes. The matrix element $\underline{S}^{he}_{\downarrow\uparrow}$ describes Andreev reflection of an incoming electron with spin parallel to the magnetisation vector, and is thus equivalent to the reflection amplitude $r^{\uparrow}_{he}$ in Ref. [98]. It is evident from the difference in electron and hole distribution functions that the charge current vanishes in electrochemical equilibrium. As a final note, it is worth mentioning that even though we have found the same qualitative expression for the charge current as that reported in the normal metal-ferromagnetic superconductor junction, we do expect quantitative differences, since $\underline{S}^{he}$ will, in general, be different from r_{he} of Ref. [98].

As advertised, the spin current is more involved. After careful evaluation, we find that it can be written as

$$\begin{aligned}
\boldsymbol{I}_s(t) = &-\frac{1}{4\pi}\int_{-\infty}^{\infty} \mathrm{d}\varepsilon \ (f_e(\varepsilon) - f_h(\varepsilon)) \left(\tilde{p}\tilde{g}\boldsymbol{m}(t) - \mathrm{Tr}\left\{ \boldsymbol{\sigma}^* (\Gamma^{he} S_0^{he\dagger} + S_0^{he} \Gamma^{he\dagger}) \right\} \right) \\
&+\frac{\hbar}{8\pi}\int_{-\infty}^{\infty} \mathrm{d}\varepsilon \ (f_e(\varepsilon) - f_h(\varepsilon)) \, \partial_\varepsilon \Big(\boldsymbol{m} \times \partial_t \boldsymbol{m} \big(\tilde{g} + 2\mathrm{Re} \sum_{m,n} \underline{S}^{he}_{\downarrow\uparrow,mn} \underline{S}^{he*}_{\uparrow\downarrow,mn} \big) \\
&\qquad\qquad + 2\partial_t \boldsymbol{m} \mathrm{Im} \sum_{m,n} \underline{S}^{he}_{\downarrow\uparrow,mn} \underline{S}^{he*}_{\uparrow\downarrow,mn} \Big) \\
&+\frac{\hbar}{4\pi}\int_{-\infty}^{\infty} \mathrm{d}\varepsilon \, \partial_\varepsilon f_e(\varepsilon) \left(\boldsymbol{m} \times \partial_t \boldsymbol{m} \mathrm{Re}\tilde{g}^{\uparrow\downarrow} + \partial_t \boldsymbol{m} \mathrm{Im}\tilde{g}^{\uparrow\downarrow} \right), \qquad (4.7)
\end{aligned}$$

where the conductance polarisation

$$\tilde{p} \equiv \frac{1}{\tilde{g}} \sum_{m,n} \left\{ \left| \underline{S}^{he}_{\downarrow\uparrow,mn} \right|^2 - \left| \underline{S}^{he}_{\uparrow\downarrow,mn} \right|^2 \right\},$$

and the generalised mixing conductance

$$\tilde{g}^{\uparrow\downarrow} \equiv \sum_{m,n} \left\{ \delta_{m,n} - \underline{S}^{ee}_{\uparrow,mn} \underline{S}^{ee*}_{\downarrow,mn} + \underline{S}^{he}_{\downarrow\uparrow,mn} \underline{S}^{he*}_{\uparrow\downarrow,mn} \right\}, \qquad (4.8)$$

are identical in form to those of Ref. [98]. The matrix Γ^{he} is a "gradient remainder" matrix introduced in paper [4], which contains contributions to the spin current that are linear in pumping frequency. This is one of the non-trivial corrections to the pumped current when the system is out of electro-chemical equilibrium, and it can be shown that

$$\begin{aligned}
\Gamma^{he} = &\, \mathrm{i}\hbar t^*_{12} \partial_\varepsilon (M_e r^A_{he}) \partial_t t_{21} + \mathrm{i}\hbar t^*_{12} \partial_\varepsilon \partial_t M_e r^A_{he} t_{21} \\
&+ \mathrm{i}\hbar t^*_{12} \partial_t M_e \partial_\varepsilon M_e^{-1} M_e r^A_{he} t_{21} - \mathrm{i}\hbar t^*_{12} M_e r^A_{he} \partial_t r_{22} \partial_\varepsilon r^A_{eh} r^*_{22} M_e r^A_{he} t_{21},
\end{aligned}$$

for our model.

When the system is in electro-chemical equilibrium, we observe that only the final line of Eq. (4.7) remains. This agrees with the pumped spin current that has previously been obtained in normal metal-ferromagnet and in normal metal-ferromagnetic superconductor junctions, albeit with quantitatively different mixing conductances.

Even though the spin current in Eq. (4.7) is unwieldy, it is possible to arrive at a simpler expression if we limit our attention to long ferromagnets. Based on the discussion of various proximity effects in Sec. 4.2, we expect reduced influence of Andreev reflections on the measured spin current as the ferromagnet increases in length. The expression for the charge current, Eq. (4.6), should remain unchanged however, since Andreev reflection is the process by which charge is transferred between the two reservoirs. To investigate how the spin current is affected when the ferromagnet is made "long", we consider ferromagnets longer than the transverse spin coherence length,

$$L_x > L_{sc} \equiv \frac{\pi}{|k_{F\uparrow} - k_{F\downarrow}|}, \tag{4.9}$$

where L_x is the length of the ferromagnet, and $k_{F\sigma}$ the Fermi wave vector of a spin-σ particle. In this limit, one disregards "mixing transmission" terms $\sim t_\sigma t^*_{-\sigma}$ [19], which simplifies the mixing conductance:

$$\tilde{g}^{\uparrow\downarrow} \to g^{\uparrow\downarrow}_{N|F} = \sum_{m,n} \left[\delta_{m,n} - \underline{r}_{\uparrow,mn}\underline{r}^*_{\downarrow,mn}\right],$$

where $\underline{r}_\sigma$ is the reflection coefficient for an electron of spin-σ impinging on the normal metal-ferromagnet interface. By inspection, one also verifies that matrix products involving the "gradient remainder" matrix are proportional to "mixing transmission" terms, and should thus be disregarded in the limit (4.9). Taken together, we arrive at the following expression for the spin current when $L_x > L_{sc}$:

$$\begin{aligned}\boldsymbol{I}_s(t) \to -\frac{1}{4\pi}\int_{-\infty}^{\infty} \mathrm{d}\varepsilon\ \left(f_e(\varepsilon) - f_h(\varepsilon)\right)\left(\tilde{p}\tilde{g}\boldsymbol{m}(t) - \hbar\boldsymbol{m}\times\partial_t\boldsymbol{m}\partial_\varepsilon\tilde{g}/2\right)\\ + \frac{\hbar}{4\pi}\int_{-\infty}^{\infty}\mathrm{d}\varepsilon\ \partial_\varepsilon f_e(\varepsilon)\left(\boldsymbol{m}\times\partial_t\boldsymbol{m}\mathrm{Re}g^{\uparrow\downarrow} + \partial_t\boldsymbol{m}\mathrm{Im}g^{\uparrow\downarrow}\right).\end{aligned}$$

In this limit, the contributions of Andreev reflections are contained in the conductance polarisation and in the energy gradient of the conductance. In electro-chemical equilibrium, both terms vanish, and the spin current is exclusively determined by the normal metal-ferromagnet interface. The charge current (4.6) remains unchanged in this limit, and will still be determined by details of the complete structure, as expected.

Bibliography

[1] Y. Tserkovnyak, H. J. Skadsem, A. Brataas, and G. E. W. Bauer. Current-induced magnetization dynamics in disordered itinerant ferromagnets. *Phys. Rev. B*, 74(14):144405, 2006.

[2] H. J. Skadsem, Y. Tserkovnyak, A. Brataas, and G. E. W. Bauer. Magnetization damping in a local-density approximation. *Phys. Rev. B*, 75(9):094416, 2007.

[3] A. K. Nguyen, H. J. Skadsem, and A. Brataas. Giant Current-Driven Domain Wall Mobility in (Ga,Mn)As. *Phys. Rev. Lett.*, 98(14):146602, 2007.

[4] H. J. Skadsem, A. Brataas, J. Martinek, and Y. Tserkovnyak. FMR and voltage induced transport in normal metal−ferromagnet−superconductor trilayers. Draft, 2009.

[5] W. Gerlach and O. Stern. Das magnetische Moment des Silberatoms. *Z. Physik A*, 9(1):353 – 355, December 1922.

[6] T. E. Phipps and J. B. Taylor. The Magnetic Moment of the Hydrogen Atom. *Phys. Rev.*, 29(2):309–320, Feb 1927.

[7] G. E. Uhlenbeck and S. Goudsmit. Replacement of the hypothesis of unmechanical coercion by a requirement for the internal condition of every electron. *Naturwissenschaften*, 13:953 – 954, 1925.

[8] P. A. M. Dirac. The Quantum Theory of the Electron. *Proc. R. Soc. Lond. A*, 117(778):610–624, February 1928.

[9] H. Kohno, G. Tatara, and J. Shibata. Microscopic Calculation of Spin Torques in Disordered Ferromagnets. *J. Phys. Soc. Jpn.*, 75(11):113706, 2006.

[10] R. A. Duine, A. S. Núñez, Jairo Sinova, and A. H. MacDonald. Functional Keldysh theory of spin torques. *Phys. Rev. B*, 75(21):214420, 2007.

[11] G. Binasch, P. Grünberg, F. Saurenbach, and W. Zinn. Enhanced magnetoresistance in layered magnetic structures with antiferromagnetic interlayer exchange. *Phys. Rev. B*, 39(7):4828–4830, Mar 1989.

[12] M. N. Baibich, J. M. Broto, A. Fert, F. Nguyen Van Dau, F. Petroff, P. Etienne, G. Creuzet, A. Friederich, and J. Chazelas. Giant Magnetoresistance of (001)Fe/(001)Cr Magnetic Superlattices. *Phys. Rev. Lett.*, 61(21):2472–2475, Nov 1988.

[13] J. Mathon. *Spin Electronics*, volume 569 of *Lecture Notes in Physics*, chapter 4, pages 71 – 88. Springer Berlin/Heidelberg, 2001.

[14] The Nobel Prize in Physics 2007: Press Release. `http://nobelprize.org/nobel_prizes/physics/laureates/2007/press.html`, October 2007.

[15] J. C. Slonczewski. Current-driven excitation of magnetic multilayers. *J. Magn. Magn. Mater.*, 159(1-2):L1 – L7, 1996.

[16] L. Berger. Emission of spin waves by a magnetic multilayer traversed by a current. *Phys. Rev. B*, 54(13):9353–9358, Oct 1996.

[17] E. B. Myers, D. C. Ralph, J. A. Katine, R. N. Louie, and R. A. Buhrman. Current-Induced Switching of Domains in Magnetic Multilayer Devices. *Science*, 285(5429):867–870, 1999.

[18] J. A. Katine, F. J. Albert, R. A. Buhrman, E. B. Myers, and D. C. Ralph. Current-Driven Magnetization Reversal and Spin-Wave Excitations in Co /Cu /Co Pillars. *Phys. Rev. Lett.*, 84(14):3149–3152, Apr 2000.

[19] M. D. Stiles and A. Zangwill. Anatomy of spin-transfer torque. *Phys. Rev. B*, 66(1):014407, Jun 2002.

[20] A. Brataas, Yu. V. Nazarov, and G. E. W. Bauer. Finite-element theory of transport in ferromagnet–normal metal systems. *Phys. Rev. Lett.*, 84(11):2481–2484, Mar 2000.

[21] A. Brataas, Yu. V. Nazarov, and G. E. W. Bauer. Spin-transport in multi-terminal normal metal-ferromagnet systems with non-collinear magnetizations. *Eur. Phys. J. B*, 22(1):99–110, 2001.

[22] X. Waintal, E. B. Myers, P. W. Brouwer, and D. C. Ralph. Role of spin-dependent interface scattering in generating current-induced torques in magnetic multilayers. *Phys. Rev. B*, 62(18):12317–12327, Nov 2000.

[23] Y. Tserkovnyak, A. Brataas, G. E. W. Bauer, and B. I. Halperin. Nonlocal magnetization dynamics in ferromagnetic heterostructures. *Rev. Mod. Phys.*, 77(4):1375–1421, Dec 2005.

[24] B. Heinrich and J. F. Cochran. Ultrathin metallic magnetic films: magnetic anisotropies and exchange interactions. *Adv. Phys.*, 42(5):523–639, October 1993.

[25] H. Kamerlingh Onnes. The resistance of pure mercury at helium temperatures. *Comm. Leiden.*, 120b, April 1911.

[26] H. Kamerlingh Onnes. The disappearance of the resistivity of mercury. *Comm. Leiden.*, 122b, May 1911.

[27] H. Kamerlingh Onnes. On the sudden change in the rate at which the resistance of mercury disappears. *Comm. Leiden.*, 124c, November 1911.

[28] M. Tinkham. *Introduction to superconductivity.* McGraw-Hill, New York, 1975.

[29] W. Meissner and R. Ochsenfeld. Ein neuer Effekt bei Eintritt der Supraleitfähigkeit. *Naturwissenschaften*, 21(44):787 – 788, November 1933.

[30] V. L. Ginzburg and L. D. Landau. On the theory of superconductivity. *Zh. Eksp. Teor. Fiz.*, 20:1064 – 1082, 1950.

[31] J. Bardeen, L. N. Cooper, and J. R. Schrieffer. Theory of superconductivity. *Phys. Rev.*, 108(5):1175–1204, Dec 1957.

[32] L. D. Landau, E. M. Lifshitz, and L. P. Pitaevskii. *Statistical Physics, Part 2.* Course of Theoretical Physics. Pergamon Press Ltd., 1980.

[33] T. L. Gilbert. A Lagrangian formulation of the gyromagnetic equation of the magnetization field. *Phys. Rev.*, 100:1243, November 1955. [abstract only; full report, *Armor Research Foundation Project No. A059*, Supplementary Report, May 1, 1956] (unpublished).

[34] T.L. Gilbert. A phenomenological theory of damping in ferromagnetic materials. *Magnetics, IEEE Transactions on*, 40(6):3443–3449, Nov. 2004.

[35] S. M. Bhagat and P. Lubitz. Temperature variation of ferromagnetic relaxation in the 3*d* transition metals. *Phys. Rev. B*, 10(1):179–185, Jul 1974.

[36] B. Heinrich. *Ultrathin Magnetic Structures III*, chapter 5: Spin Relaxation in Magnetic Metallic Layers and Multilayers, pages 143 – 210. Fundamentals of Nanomagnetism. Springer Verlag, Heidelberg, 2005.

[37] A. H. Mitchell. Ferromagnetic Relaxation by the Exchange Interaction between Ferromagnetic Electrons and Conduction Electrons. *Phys. Rev.*, 105(5):1439–1444, Mar 1957.

[38] B. Heinrich, D. Fraitová, and V. Kamberský. The influence of *s-d* exchange on relaxation of magnons in metals. *Phys. Status Solidi*, 23:501 – 507, July 1967.

[39] R. J. Elliott. Theory of the Effect of Spin-Orbit Coupling on Magnetic Resonance in Some Semiconductors. *Phys. Rev.*, 96(2):266–279, Oct 1954.

[40] V. Kamberský. On the Landau-Lifshitz relaxation in ferromagnetic metals. *Can. J. Phys.*, 48(24):2906 – 2911, June 1970.

[41] V. Korenman and R. E. Prange. Anomalous damping of spin waves in magnetic metals. *Phys. Rev. B*, 6(7):2769–2777, Oct 1972.

[42] B. Heinrich, D. J. Meredith, and J. F. Cochran. Wave number and temperature dependent Landau-Lifshitz damping in nickel. *J. Appl. Phys.*, 50(B11):7726–7728, 1979.

[43] J. F. Cochran and B. Heinrich. Microwave transmission through ferromagnetic metals. *IEEE Trans. Magn.*, 16(5):660 – 665, September 1980.

[44] V. Kamberský. On ferromagnetic resonance damping in metals. *Czech. J. Phys., Sect. B*, 26(12):1366 – 1383, December 1976.

[45] K. Gilmore, Y. U. Idzerda, and M. D. Stiles. Identification of the Dominant Precession-Damping Mechanism in Fe, Co, and Ni by First-Principles Calculations. *Phys. Rev. Lett.*, 99(2):027204, 2007.

[46] M. Tsoi, A. G. M. Jansen, J. Bass, W.-C. Chiang, V. Tsoi, and P. Wyder. Generation and detection of phase-coherent current-driven magnons in magnetic multilayers. *Nature*, 406:46–48, July 2000.

[47] S. I. Kiselev, J. C. Sankey, I. N. Krivorotov, N. C. Emley, R. J. Schoelkopf, R. A. Buhrman, and D. C. Ralph. Microwave oscillations of a nanomagnet driven by a spin-polarized current. *Nature*, 425:380–383, September 2003.

[48] B. Özyilmaz, A. D. Kent, D. Monsma, J. Z. Sun, M. J. Rooks, and R. H. Koch. Current-Induced Magnetization Reversal in High Magnetic Fields in $Co/Cu/Co$ Nanopillars. *Phys. Rev. Lett.*, 91(6):067203, Aug 2003.

[49] I. N. Krivorotov, N. C. Emley, J. C. Sankey, S. I. Kiselev, D. C. Ralph, and R. A. Buhrman. Time-Domain Measurements of Nanomagnet Dynamics Driven by Spin-Transfer Torques. *Science*, 307(5707):228–231, 2005.

[50] Ya. B. Bazaliy, B. A. Jones, and Shou-Cheng Zhang. Modification of the Landau-Lifshitz equation in the presence of a spin-polarized current in colossal- and giant-magnetoresistive materials. *Phys. Rev. B*, 57(6):R3213–R3216, Feb 1998.

[51] Z. Li and S. Zhang. Domain-wall dynamics and spin-wave excitations with spin-transfer torques. *Phys. Rev. Lett.*, 92(20):207203, May 2004.

[52] Z. Li and S. Zhang. Domain-wall dynamics driven by adiabatic spin-transfer torques. *Phys. Rev. B*, 70(2):024417, Jul 2004.

[53] G. Tatara and H. Kohno. Theory of Current-Driven Domain Wall Motion: Spin Transfer versus Momentum Transfer. *Phys. Rev. Lett.*, 92(8):086601, Feb 2004.

[54] A. Thiaville, Y. Nakatani, J. Miltat, and N. Vernier. Domain wall motion by spin-polarized current: a micromagnetic study. *J. Appl. Phys.*, 95(11):7049–7051, 2004.

[55] A. Yamaguchi, T. Ono, S. Nasu, K. Miyake, K. Mibu, and T. Shinjo. Real-Space Observation of Current-Driven Domain Wall Motion in Submicron Magnetic Wires. *Phys. Rev. Lett.*, 92(7):077205, Feb 2004.

[56] M. Kläui, C. A. F. Vaz, J. A. C. Bland, W. Wernsdorfer, G. Faini, E. Cambril, L. J. Heyderman, F. Nolting, and U. Rüdiger. Controlled and Reproducible Domain Wall Displacement by Current Pulses Injected into Ferromagnetic Ring Structures. *Phys. Rev. Lett.*, 94(10):106601, Mar 2005.

[57] S. Zhang and Z. Li. Roles of nonequilibrium conduction electrons on the magnetization dynamics of ferromagnets. *Phys. Rev. Lett.*, 93(12):127204, Sep 2004.

[58] N. L. Schryer and L. R. Walker. The motion of 180° domain walls in uniform dc magnetic fields. *J. Appl. Phys.*, 45(12):5406–5421, 1974.

[59] A. Thiaville, Y. Nakatani, J. Miltat, and Y. Suzuki. Micromagnetic understanding of current-driven domain wall motion in patterned nanowires. *Europhys. Lett.*, 69(6):990–996, 2005.

[60] J. Rammer and H. Smith. Quantum field-theoretical methods in transport theory of metals. *Rev. Mod. Phys.*, 58(2):323–359, Apr 1986.

[61] L. V. Keldysh. Diagram technique for nonequilibrium processes. *Zh. Eksp. Teor. Fiz.*, 47:1515–1527, 1964.

[62] M. Yamanouchi, D. Chiba, F. Matsukura, and H. Ohno. Current-induced domain-wall switching in a ferromagnetic semiconductor structure. *Nature*, 428(6982):539 – 542, April 2004.

[63] M. Yamanouchi, D. Chiba, F. Matsukura, T. Dietl, and H. Ohno. Velocity of Domain-Wall Motion Induced by Electrical Current in the Ferromagnetic Semiconductor (Ga,Mn)As. *Phys. Rev. Lett.*, 96(9):096601, 2006.

[64] A. K. Nguyen, R. V. Shchelushkin, and A. Brataas. Intrinsic Domain-Wall Resistance in Ferromagnetic Semiconductors. *Phys. Rev. Lett.*, 97(13):136603, 2006.

[65] A. F. Andreev. Thermal conductivity of the intermediate state of superconductors. *Zh. Eksp. Teor. Fiz.*, 46:1823–1828, 1964. [Sov. Phys. JETP **19**, 1228 (1964)].

[66] C. W. J. Beenakker. Random-matrix theory of quantum transport. *Rev. Mod. Phys.*, 69(3):731–808, Jul 1997.

[67] G. E. Blonder, M. Tinkham, and T. M. Klapwijk. Transition from metallic to tunneling regimes in superconducting microconstrictions: Excess current, charge imbalance, and supercurrent conversion. *Phys. Rev. B*, 25(7):4515–4532, Apr 1982.

[68] B. Pannetier and H. Courtois. Andreev Reflection and Proximity effect. *J. Low Temp. Phys.*, 118:599 – 615, 2000.

[69] A. I. Buzdin. Proximity effects in superconductor-ferromagnet heterostructures. *Rev. Mod. Phys.*, 77(3):935–976, Sep 2005.

[70] P. G. de Gennes. Boundary Effects in Superconductors. *Rev. Mod. Phys.*, 36(1):225–237, Jan 1964.

[71] W. Belzig, C. Bruder, and G. Schön. Local density of states in a dirty normal metal connected to a superconductor. *Phys. Rev. B*, 54(13):9443–9448, Oct 1996.

[72] B. D. Josephson. Possible new effects in superconductive tunnelling. *Phys. Lett.*, 1(7):251 – 253, 1962.

[73] K. K. Likharev. Superconducting weak links. *Rev. Mod. Phys.*, 51(1):101–159, Jan 1979.

[74] The Nobel Prize in Physics 1973: Press Release. `http://nobelprize.org/nobel_prizes/physics/laureates/1973/press.html`, October 1973.

[75] S. S. Saxena, P. Agarwal, K. Ahilan, F. M. Grosche, R. K. W. Haselwimmer, M. J. Steiner, E. Pugh, I. R. Walker, S. R. Julian, P. Monthoux, G. G. Lonzarich, A. Huxley, I. Sheikin, D. Braithwaite, and J. Flouquet. Superconductivity on the border of itinerant-electron ferromagnetism in UGe_2. *Nature*, 406(6796):587 – 592, August 2000.

[76] C. Pfleiderer, M. Uhlarz, S. M. Hayden, R. Vollmer, H. v. Lohneysen, N. R. Bernhoeft, and G. G. Lonzarich. Coexistence of superconductivity and ferromagnetism in the *d*-band metal $ZrZn_2$. *Nature*, 412(6842):58 – 61, July 2001.

[77] D. Aoki, A. Huxley, E. Ressouche, D. Braithwaite, J. Flouquet, J.-P. Brison, E. Lhotel, and C. Paulsen. Coexistence of superconductivity and ferromagnetism in URhGe. *Nature*, 413(6856):613 – 616, October 2001.

[78] M. J. M. de Jong and C. W. J. Beenakker. Andreev reflection in ferromagnet-superconductor junctions. *Phys. Rev. Lett.*, 74(9):1657–1660, Feb 1995.

[79] A. Buzdin. Density of states oscillations in a ferromagnetic metal in contact with a superconductor. *Phys. Rev. B*, 62(17):11377–11379, Nov 2000.

[80] T. Kontos, M. Aprili, J. Lesueur, and X. Grison. Inhomogeneous Superconductivity Induced in a Ferromagnet by Proximity Effect. *Phys. Rev. Lett.*, 86(2):304–307, Jan 2001.

[81] A. I. Larkin and Yu. N. Ovchinnikov. Nonuniform state of superconductors. *Zh. Eksp. Teor. Fiz.*, 47(3):1136 – 1146, 1964. [Sov. Phys. JETP **20**, 762 (1965)].

[82] P. Fulde and R. A. Ferrell. Superconductivity in a Strong Spin-Exchange Field. *Phys. Rev.*, 135(3A):A550–A563, Aug 1964.

[83] L. N. Bulaevskiĭ, V. V. Kuziĭ, and A. A. Sobyanin. Superconducting system with weak coupling to the current in the ground state. *Zh. Eksp. Teor. Fiz.*, 25:314, 1977. [JETP Lett. **25**, 290 (1977)].

[84] A. I. Buzdin, L. N. Bulaevskiĭ, and S. V. Panyukov. Critical-current oscillations as a function of the exchange field and thickness of the ferromagnetic metal (F) in an S-F-S Josephson junction. *Zh. Eksp. Teor. Fiz.*, 35:147 – 148, 1982. [JETP Lett. **35**, 178 (1982)].

[85] V. V. Ryazanov, V. A. Oboznov, A. Yu. Rusanov, A. V. Veretennikov, A. A. Golubov, and J. Aarts. Coupling of Two Superconductors through a Ferromagnet: Evidence for a π Junction. *Phys. Rev. Lett.*, 86(11):2427–2430, Mar 2001.

[86] M. D. Lawrence and N. Giordano. Weak-localization-like effects in superconductor - ferromagnet - superconductor structures. *J. Phys.: Condens. Matter*, 8(39):L563–L568, 1996.

[87] M. Giroud, H. Courtois, K. Hasselbach, D. Mailly, and B. Pannetier. Superconducting proximity effect in a mesoscopic ferromagnetic wire. *Phys. Rev. B*, 58(18):R11872–R11875, Nov 1998.

[88] V. T. Petrashov, I. A. Sosnin, I. Cox, A. Parsons, and C. Troadec. Giant Mutual Proximity Effects in Ferromagnetic/Superconducting Nanostructures. *Phys. Rev. Lett.*, 83(16):3281–3284, Oct 1999.

[89] F. S. Bergeret, A. F. Volkov, and K. B. Efetov. Long-Range Proximity Effects in Superconductor-Ferromagnet Structures. *Phys. Rev. Lett.*, 86(18):4096–4099, Apr 2001.

[90] A. Kadigrobov, R. I. Shekhter, and M. Jonson. Quantum spin fluctuations as a source of long-range proximity effects in diffusive ferromagnet-super conductor structures. *Europhys. Lett.*, 54(3):394–400, 2001.

[91] F. S. Bergeret, A. F. Volkov, and K. B. Efetov. Odd triplet superconductivity and related phenomena in superconductor-ferromagnet structures. *Rev. Mod. Phys.*, 77(4):1321–1373, Nov 2005.

[92] Manuel Houzet. Ferromagnetic Josephson Junction with Precessing Magnetization. *Phys. Rev. Lett.*, 101(5):057009, 2008.

[93] Y. Tserkovnyak and A. Brataas. Shot noise in ferromagnet–normal metal systems. *Phys. Rev. B*, 64(21):214402, Oct 2001.

[94] M. Büttiker. Scattering theory of current and intensity noise correlations in conductors and wave guides. *Phys. Rev. B*, 46(19):12485–12507, Nov 1992.

[95] W. Belzig, F. K. Wilhelm, C. Bruder, G. Schön, and A. D. Zaikin. Quasiclassical Green's function approach to mesoscopic superconductivity. *Superlattices Microstruct.*, 25(5-6):1251 – 1288, 1999.

[96] M. Moskalets and M. Büttiker. Adiabatic quantum pump in the presence of external ac voltages. *Phys. Rev. B*, 69(20):205316, May 2004.

[97] M. Büttiker and M. Moskalets. *Mathematical Physics of Quantum Mechanics*, volume 690 of *Lecture Notes in Physics*, chapter 5, pages 33 – 44. Springer Verlag, Heidelberg, 2006.

[98] A. Brataas and Y. Tserkovnyak. Spin and Charge Pumping by Ferromagnetic-Superconductor Order Parameters. *Phys. Rev. Lett.*, 93(8):087201, Aug 2004.

Paper [1]

"Current-induced magnetization dynamics in disordered itinerant ferromagnets"

Phys. Rev. B **74**, 144405 (2006)

Is not included due to copyright

Paper [2]

"Magnetization damping in a local-density approximation"

Phys. Rev. B **75**, 094416 (2007)

Is not included due to copyright

Paper [3]

"Giant Current-Driven Domain Wall Mobility in (Ga,Mn)As"

Phys. Rev. Lett. **98**, 146602 (2007)

Is not included due to copyright

Paper [4]

"FMR and voltage induced transport in normal metal–ferromagnet–superconductor trilayers"

Manuscript to be submitted to Phys. Rev. B (2009)

FMR and voltage induced transport in normal metal–ferromagnet–superconductor trilayers

Hans Joakim Skadsem and Arne Brataas
Department of Physics, Norwegian University of Science and Technology, NO-7491 Trondheim, Norway

Jan Martinek
Institute of Molecular Physics, Polish Academy of Science, 60-179 Poznań, Poland

Yaroslav Tserkovnyak
Department of Physics and Astronomy, University of California, Los Angeles, California 90095, USA

We study charge and spin transport in normal metal-ferromagnet-superconductor trilayers induced by bias voltage and/or magnetization precession. Transport properties are discussed in terms of time-dependent scattering theory. We assume that the superconducting gap is small on the energy scale set by the Fermi energy and the ferromagnetic exchange splitting, and compute the non-equilibrium charge and spin current response to first order in precession frequency, in the presence of a finite applied voltage. We find that both charge current and longitudinal spin current are unaffected by the precessing magnetization, while the pumped transverse spin current is determined by spin-dependent conductances and details of the electron-hole scattering matrix. A simplified expression for the transverse spin current is derived for structures where the ferromagnet is longer than the transverse spin coherence length.

PACS numbers: 74.25.Fy,74.78.Na,85.75.-d,72.25.-b

I. INTRODUCTION

Experimental and theoretical studies of spin polarized transport in hybrid magnetic nanostructures is a frontier in mesoscopic physics. The most prominent example of conceptual, technological, and commercial impact is the giant magnetoresistance effect utilized in magnetic information storage devices. In order to gain a deeper understanding of spin and charge transport, and to enhance circuit functionality and efficiency, more complex structures are fabricated and studied. In recent years, hybrid nanoscale circuits containing normal conductors, ferromagnets, and superconductors have been realized. These structures allow observation and understanding of competing mechanisms of electron-electron interactions.

The simultaneous existence of ferromagnetism and superconductivity is rare. In ferromagnets, the exchange interaction lifts the spin-degeneracy and induces an itinerant spin polarization. In s-wave superconductors, on the other hand, electrons with anti-parallel spins form Cooper pairs. In conventional ferromagnets (Fe, Ni, Co, and alloys thereof), the large exchange interaction efficiently dephases electron-hole pairs, and eliminates singlet superconducting correlations over distances larger than the ferromagnetic coherence length. This would suggest a short-range superconducting proximity effect in transition metal ferromagnets.[1,2] Such a simple picture cannot explain recent measurements on Co and Ni ferromagnets coupled to Al superconductors, however, where a substantial resistance drop was observed at the onset of superconductivity.[3,4] The simple picture also fails to explain the long-range superconducting proximity effect recently observed via the Josephson supercurrent through a half-metallic ferromagnet.[5] Subsequent theoretical work show that induced triplet superconducting correlations give rise to long ranged proximity effect in transition metal ferromagnets.[6,7] Triplet superconducting correlations are insensitive to the pair-breaking exchange interaction and exhibit a longer coherence length, similar to that of superconducting correlations in normal metals. It is now established that spin-flip processes in a ferromagnet can convert singlet into triplet pair correlations. A spatially inhomogeneous magnetization texture[8] or magnons[9–11] are examples of spin-flip sources that are able to induce long ranged triplet correlations.

In this report, we focus our attention on the influence of magnons on the transport properties in normal metal-ferromagnet-superconductor systems. Even normal metal-ferromagnet systems without superconductors exhibit intriguing physics, and especially the interaction between spin and charge currents and the magnetic order parameter in such structures have attracted tremendous interest. For instance, a non-collinear spin flow towards a ferromagnet exerts a torque on the magnetization, a spin transfer torque, that can excite the magnetization and even induce steady state, precessional motion of the ferromagnetic order parameter.[12,13] The inverse effect is also of significant interest: A precessing ferromagnet in electrochemical equilibrium with its environment, acts as a "spin battery" by emitting (or "pumping") pure spin currents into neighboring materials.[14] When emitted spins are dissipated in adjacent materials, spin pumping enhances magnetic dissipation in the precessing ferromagnet, and thus increases observed linewidths in FMR experiments.[15]

Some ideas from spin transfer physics in normal metal-ferromagnet structures were recently used to

study superconductor-ferromagnet systems. A FMR experiment[16] and the following theoretical analysis[17] have shown how spin pumping can be used to visualize proximity effects and spin relaxation processes inside the superconductor. In essence, in metallic contacts, ferromagnetic correlations reduce the superconducting order parameter close to the layer interface, enabling pumped sub-gap electrons to enter and deposit spin in the superconductor. This is a prime example of how the inverse proximity effect affects the FMR linewidth broadening when typical spin-flip lengths are comparable to the superconducting coherence length.[18]

We direct our attention to a different aspect of the interplay between magnetization and carrier dynamics in ferromagnet-superconductor structures. In contrast to the works mentioned above, where the magnetization dynamics have been the primary concern, we will consider how a precessing magnetization and an applied voltage bias induce spin and charge currents in a normal metal-ferromagnet-superconductor (N|F|S) trilayer. The computed charge currents can be measured directly, whereas spin currents can possibly be measured by its dissipative effect on the precessing ferromagnet, its spin transfer torque effect on a second ferromagnet, or via spin-filtering as a charge buildup on another ferromagnet.[14] Related to our work, sub-gap transport properties have recently been studied in a normal metal-ferromagnetic superconductor structure.[19] It was shown how superconducting correlations, namely Andreev reflections at the layer interface, add features to the results of spin and charge pumping in normal metal-ferromagnet systems. In this report, we also consider how pumping in the N|F|S trilayer is related to pumping in the normal metal-ferromagnetic superconductor system.

Diffusive transport in hybrid superconductor-normal metal systems, is usually formulated within a quasiclassical description.[20] Although this description give qualitative insight into transport properties of superconductor-ferromagnet systems,[8,11] the formalism is limited to ferromagnets with exchange interactions much smaller than the Fermi energy. Thus, a quasiclassical description cannot be used to quantitatively study transport in transition metal ferromagnets Fe, Ni and Co used in experiments. For this reason, we adopt the scattering theory to transport.[21]

Scattering theory has proven most useful in the study of stationary charge and spin currents in magnetoelectronic structures,[22] and the time-dependent generalization has successfully been applied to describe parametric pumping of charge[23–25] and spin currents.[14] For the N|F|S structure under consideration, we derive charge- and spin currents in the normal metal conductor in response to a slowly precessing ferromagnetic exchange field and applied bias voltage. We focus on sub-gap energies, and how Andreev scattering contributes to the conductivites of the currents. In electrochemical equilibrium, we make contact with the results for pumping in normal metal-ferromagnetic superconductor structures.[19] We proceed by detailing how time- and energy gradients of the total scattering matrix contribute to non-equilibrium pumped currents, and find that both charge and longitudinal spin currents are unaffected by the precessing magnetization. Finally, we consider non-equilibrium charge and spin currents for trilayers where the ferromagnetic region is longer than the transverse spin coherence length.

This paper is organized in the following way: The N|F|S system is described in Sec. II. In Sec. III, we use time-dependent scattering theory to derive general expressions for charge and spin currents to first order in pumping frequency. The total scattering matrix for the system is then invoked in Sec. IV to obtain non-equilibrium pumped currents. Our conclusions are in Sec. V.

II. MODEL DESCRIPTION

The system is sketched in Fig. 1. It consists of a superconductor (S) in series with a ferromagnet (F) and a normal metal lead (N_1). N_1 is ideally coupled to a normal metal reservoir (N_{res}). We assume N_{res} and S to be in local thermal equilibrium, and denote a possible chemical potential difference between the normal and the superconducting side as $\mu_N - \mu_S = eV$. Spin-orbit interactions are disregarded, and the ferromagnetic order parameter is assumed to be homogeneous and with a fixed magnitude Δ_{xc} inside F. Its direction is along the time-dependent unit vector $\boldsymbol{m}(t) = (\sin\theta(t)\cos\Omega t, \sin\theta(t)\sin\Omega t, \cos\theta(t))$. The precessing magnetization serves as the pumping parameter in the system.

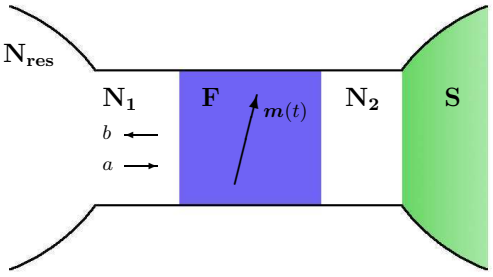

FIG. 1: A ferromagnetic scattering region (F) is connected to a superconductor (S) and a normal metal reservoir (N_{res}) via two normal metal leads (N_1 and N_2). Amplitudes of outgoing (incoming) carrier states are given by b (a).

We focus on sub-gap transport properties. Thus, possible scattering processes include Andreev reflections at the F|S interface[26] and spin-dependent normal scattering inside F. Following a standard procedure,[27] the scattering problem is greatly simplified by spatially separating regions where scattering processes occur. This is achieved

by inserting a fictitious normal metal lead (N_2) between F and S. We assume that N_2 is longer than the Fermi wavelength, so that asymptotic, plane wave solutions are applicable in this region. The total scattering matrix will be a concatenation of the scattering matrices for $N_1|F|N_2$ and for Andreev reflections at the $N_2|S$ interface. Transport between F and S is mediated by the ballistic N_2 lead.

The singlet superconductor is described by the BCS Hamiltonian

$$\hat{\mathcal{H}} = \sum_{\sigma=\uparrow,\downarrow} \int \mathrm{d}\boldsymbol{r}\ \hat{\Psi}^\dagger_\sigma(\boldsymbol{r}) H_0(\boldsymbol{r}) \hat{\Psi}_\sigma(\boldsymbol{r}) + \int \mathrm{d}\boldsymbol{r}\ \left\{ \Delta(\boldsymbol{r}) \hat{\Psi}^\dagger_\uparrow(\boldsymbol{r}) \hat{\Psi}^\dagger_\downarrow(\boldsymbol{r}) + \Delta^*(\boldsymbol{r}) \hat{\Psi}_\downarrow(\boldsymbol{r}) \hat{\Psi}_\uparrow(\boldsymbol{r}) \right\}, \quad (1)$$

where H_0 is the normal state, single-particle Hamiltonian and $\Delta(\boldsymbol{r})$ the superconducting gap. We model the gap by a step function, $\Delta(\boldsymbol{r}) = \Delta \mathrm{e}^{\mathrm{i}\phi}\Theta(x)$, where the phase ϕ is constant, and x is the coordinate perpendicular to the $N_2|S$ interface. We take the Fermi energy E_F to be the largest energy scale, and focus on the situation where $eV \leq \Delta \ll \Delta_{xc}, E_F$. The Hamiltonian (1) is diagonalized by the following Bogoliubov transformation[28]

$$\hat{\Psi}_\sigma(\boldsymbol{r}) = \sum_n \left\{ \hat{\gamma}_n u_n(\boldsymbol{r}, \sigma) + \hat{\gamma}^\dagger_n v^*_n(\boldsymbol{r}, \sigma) \right\}, \quad (2)$$

where $\hat{\gamma}^{(\dagger)}_n$ are quasiparticle annihilation (creation) operators that satisfy the fermionic anti-commutation relation

$$\{\hat{\gamma}_m, \hat{\gamma}^\dagger_n\} = \delta_{m,n}. \quad (3)$$

The transformation (2) results in a matrix equation for the quasiparticle eigenfunctions u_n and v_n:

$$\begin{pmatrix} H_0(\boldsymbol{r}) & \mathrm{i}\Delta(\boldsymbol{r})\sigma^y \\ -\mathrm{i}\Delta^*(\boldsymbol{r})\sigma^y & -H_0^*(\boldsymbol{r}) \end{pmatrix} \begin{pmatrix} u_n(\boldsymbol{r}) \\ v_n(\boldsymbol{r}) \end{pmatrix} = \varepsilon_n \begin{pmatrix} u_n(\boldsymbol{r}) \\ v_n(\boldsymbol{r}) \end{pmatrix}. \quad (4)$$

The quasiparticle excitation energy ε_n is measured with respect to the chemical potential of the superconductor, which is set to zero. σ^y is a Pauli matrix operating in spin space. The Bogoliubov-de Gennes Hamiltonian (4) is the starting point when we in Sec. III B derive the appropriate reflection amplitudes for quasiparticles impinging on the superconductor interface.

III. TIME-DEPENDENT SCATTERING THEORY

We now focus on the time-dependent scattering theory for the N|F|S structure in Fig. 1, apply the general framework established in Refs. 14,23–25,29, and make use of the scattering theory for hybrid superconductor-normal metal structures discussed in Refs. 27,30. We find it most convenient to study a slowly precessing magnetization by a scattering matrix expressed in the Wigner representation,[20] making the derivation of pumped currents similar to that carried out for normal systems in Refs. 31,32.

In order to describe a scattering potential of arbitrary time-dependence, we start by considering the two-time scattering matrix $\mathcal{S}(t, t')$, that relates annihilation operators between states outgoing and incoming from the scattering region:

$$\hat{b}_\alpha(t) = \sum_\beta \int \mathrm{d}t'\ \mathcal{S}_{\alpha\beta}(t, t') \hat{a}_\beta(t'). \quad (5)$$

As indicated in Fig. 1, $\hat{b}_\alpha$ ($\hat{a}_\alpha$) annihilates outgoing (incoming) state α. α labels electron-hole Nambu space index, spin and transverse wave-guide number. We assume that the reservoirs connected to the scattering region are in local thermal equilibrium, and that incoming carriers from the normal metal reservoir fulfill

$$\langle \hat{a}^\dagger_\alpha(\varepsilon) \hat{a}_{\alpha'}(\varepsilon') \rangle = \delta_{\alpha,\alpha'} \delta(\varepsilon - \varepsilon') f_\alpha(\varepsilon), \quad (6)$$

where the brackets indicate a quantum and statistical average, and

$$f_{e(h)}(\varepsilon) = f_0(\varepsilon - \sigma^{e(h)} eV) = \left[1 + \mathrm{e}^{(\varepsilon - \sigma^{e(h)} eV)/k_B T} \right]^{-1}, \quad (7)$$

where $\sigma^{e(h)} = +(-)1$, and $f_{e(h)}(\varepsilon)$ is the Fermi-Dirac distribution of incoming electrons (holes) at a charge bias eV. We will now proceed by computing charge and spin currents in the system.

A. Matrix current

We seek the right-going charge and spin currents in normal metal lead 1, and start by introducing the matrix current[33]

$$\hat{I}_{1,\alpha\beta}(t) = 2\pi e \tau^z_{\alpha\alpha} \left(\hat{a}^\dagger_\beta(t) \hat{a}_\alpha(t) - \hat{b}^\dagger_\beta(t) \hat{b}_\alpha(t) \right), \quad (8)$$

where e is the electronic charge, and τ^z is a Pauli matrix in electron-hole space:

$$\tau^z = \begin{pmatrix} 1 & 0 \\ 0 & -1 \end{pmatrix}. \quad (9)$$

Charge and spin currents are obtained from the matrix current (8) as follows:

$$I_c(t) = \sum_\alpha \langle \hat{I}_{1,\alpha\alpha}(t) \rangle, \quad (10)$$

and

$$\boldsymbol{I}_s(t) = \frac{1}{2e} \sum_{\alpha,\beta} \boldsymbol{\rho}_{\alpha\beta} \langle \hat{I}_{1,\beta\alpha}(t) \rangle, \quad (11)$$

respectively. Summations run over electron-hole, spin and mode space, and $\boldsymbol{\rho}$ is a matrix with diagonal structure in electron-hole space:

$$\boldsymbol{\rho}_{\alpha\beta} \equiv \begin{pmatrix} \boldsymbol{\sigma}_{\alpha\beta} & 0 \\ 0 & \boldsymbol{\sigma}^*_{\alpha\beta} \end{pmatrix}, \tag{12}$$

and with a vector of the Pauli matrices and their complex conjugates, as the diagonal elements.

For a slowly oscillating scatterer, it is convenient to express the scattering matrix in the Wigner representation[20,31,32]

$$\mathcal{S}_{\alpha\beta}(t,t') = \int_0^\infty \frac{\mathrm{d}\varepsilon}{2\pi} \mathrm{e}^{-\mathrm{i}\varepsilon(t-t')} \mathcal{S}_{\alpha\beta}\left(\varepsilon; \frac{t+t'}{2}\right). \tag{13}$$

In this representation, the matrix current is:

$$\langle \hat{I}_{1,\alpha\beta}(t)\rangle = \frac{e}{2\pi}\tau^z_{\alpha\alpha}\Big\{\delta_{\alpha,\beta}\int_0^\infty \mathrm{d}\varepsilon\, f_\alpha(\varepsilon) - \sum_\gamma \int_{-\infty}^\infty \mathrm{d}\tau\, \mathrm{d}T \int_0^\infty \frac{\mathrm{d}\varepsilon_1\, \mathrm{d}\varepsilon_2}{2\pi} f_\gamma(\tau) \\ \times \mathrm{e}^{-\mathrm{i}\varepsilon_1(T-\tau/2)}\mathrm{e}^{\mathrm{i}\varepsilon_2(T+\tau/2)} \mathcal{S}_{\alpha\gamma}\left(\varepsilon_2; t+\frac{T+\tau/2}{2}\right)\mathcal{S}^*_{\beta\gamma}\left(\varepsilon_1; t+\frac{T-\tau/2}{2}\right)\Big\}. \tag{14}$$

The current is expressed in terms of the center and relative time coordinates $T = (t'+t'')/2$ and $\tau = t''-t'$, and the Fourier transform of the distribution function

$$f_\gamma(\tau) \equiv \int_0^\infty \frac{\mathrm{d}\varepsilon}{2\pi}\mathrm{e}^{-\mathrm{i}\varepsilon\tau} f_\gamma(\varepsilon). \tag{15}$$

When the scattering matrix $\mathcal{S}(\varepsilon;t)$ is a concatenation of multiple time-dependent scattering elements, the Wigner representation of $\mathcal{S}$ will also be an infinite sum of time and energy gradients.[20] In the *adiabatic* approximation, we assume the scattering matrix evolves on a much longer timescale than the typical dwell times of particles inside the scattering region. In this regime, we formally expand $\mathcal{S}$ as[34]

$$\mathcal{S}(\varepsilon;t) = S_0(\varepsilon;t) + A(\varepsilon;t) + \mathcal{O}(\partial_t^2 S_0) \tag{16}$$

where S_0 is the "frozen" or instantaneous scattering matrix, and the matrix A represents all first-order gradient corrections to S_0 resulting from the concatenation of time-dependent scattering elements that describe the device. Unitarity of $\mathcal{S}$ to all orders in time- and energy-gradients implies[34]

$$S_0 A^\dagger + A S_0^\dagger = \frac{\mathrm{i}}{2}\left(\partial_t S_0 \partial_\varepsilon S_0^\dagger - \partial_\varepsilon S_0 \partial_t S_0^\dagger\right) \equiv \frac{1}{2} P\left\{S_0; S_0^\dagger\right\}, \tag{17}$$

where a Poisson bracket has been defined to ease the notation. In the following, scattering matrix arguments $(\varepsilon;t)$ are omitted in places where there is no risk of confusion.

To obtain a local (in time) expression for the matrix current (14), we Taylor expand $\mathcal{S}$ to first order in time derivatives, and obtain the matrix current

$$\langle \hat{I}_{1,\alpha\beta}(t)\rangle = \frac{e}{2\pi}\tau^z_{\alpha\alpha}\sum_\gamma \int_0^\infty \mathrm{d}\varepsilon \Big\{ \left(f_\alpha(\varepsilon) - f_\gamma(\varepsilon)\right)\left(S_{0,\alpha\gamma}S^*_{0,\beta\gamma} + A_{\alpha\gamma}S^*_{0,\beta\gamma} + S_{0,\alpha\gamma}A^*_{\beta\gamma} - \frac{1}{2}P\left\{S_{0,\alpha\gamma}; S^*_{0,\beta\gamma}\right\}\right) \\ + \frac{\mathrm{i}}{2}\left(-\partial_\varepsilon f_\gamma(\varepsilon)\right)\left(S_{0,\alpha\gamma}\partial_t S^*_{0,\beta\gamma} - \partial_t S_{0,\alpha\gamma}S^*_{0,\beta\gamma}\right)\Big\} + \mathcal{O}\left(\partial_t^2 S_0\right) \tag{18}$$

where Eqs. (16) and (17) have been used. The matrix current in Eq. (18) is *exact* to first order in frequency of the pumping parameter.

Finally, we observe that in the absence of a voltage bias, the gradient corrections to the frozen scattering matrix, represented by A, vanish from the matrix current. In electro-chemical equilibrium, when $V = 0$, $f_e(\varepsilon) = f_h(\varepsilon)$, the first line of Eq. (18) vanishes, and the pumped current is determined by the frozen scattering matrix. Naturally, the same is also true for the time-dependent theory based on Floquet scattering matrices.[25]

B. Scattering matrix for a N|F|S structure

In this section, the scattering matrix formalism derived for N|S structures[27] is applied to our N|F|S trilayer. As described in Sec. II, the scattering description of a N|F|S structure is greatly simplified by inserting a fictitious normal metal lead (N_2) between the two scattering regions, thereby spatially separating spin-dependent scattering in F and Andreev reflection at the N_2|S interface.[27] The scattering matrix S_F, describing the disordered ferromagnetic region, is block-diagonal in electron-hole space. We write S_F as

$$S_F(\varepsilon;t) = \begin{pmatrix} s_F(\varepsilon;t) & 0 \\ 0 & s_F(-\varepsilon;t)^* \end{pmatrix}, \tag{19}$$

where the diagonal elements are

$$s_F = \begin{pmatrix} r_{11} & t_{12} \\ t_{21} & r_{22} \end{pmatrix}. \tag{20}$$

Here, r_{ii} and t_{ij} are matrices in spin-space that describe reflection of an incoming electron in lead i, and transmission of an electron from lead j to lead i, respectively.

Electrons and holes with opposite spins are coupled by Andreev reflection at the superconductor interface, where an incoming electron (hole) is reflected as a hole (electron) with reversed spin direction. The reflection amplitudes are derived by matching propagating wave functions in N_2 with evanescent wave functions in the superconductor. The resulting scattering matrix reads[27,35]

$$r^A = \begin{pmatrix} 0 & r^A_{eh} \\ r^A_{he} & 0 \end{pmatrix} = \begin{pmatrix} 0 & \mathrm{i}\alpha\sigma^y \mathrm{e}^{\mathrm{i}\phi} \\ -\mathrm{i}\alpha\sigma^y \mathrm{e}^{-\mathrm{i}\phi} & 0 \end{pmatrix}, \tag{21}$$

where $\alpha = \exp\left[-\mathrm{i}\arccos(\varepsilon/\Delta)\right]$.

The total scattering matrix of the N|F|S structure is a concatenation of S_F and r^A, and in terms of the frozen scattering matrices, we obtain the familiar results[27,30]

$$\begin{aligned} S_0^{ee}(\varepsilon;t) &= r_{11}(\varepsilon) \\ &\quad + t_{12}(\varepsilon) r^A_{eh}(\varepsilon) r^*_{22}(-\varepsilon) M_e(\varepsilon) r^A_{he}(\varepsilon) t_{21}(\varepsilon), && \text{(22a)} \\ S_0^{hh}(\varepsilon;t) &= r^*_{11}(-\varepsilon) \\ &\quad + t^*_{12}(-\varepsilon) r^A_{he}(\varepsilon) r_{22}(\varepsilon) M_h(\varepsilon) r^A_{eh}(\varepsilon) t^*_{21}(-\varepsilon), && \text{(22b)} \\ S_0^{eh}(\varepsilon;t) &= t_{12}(\varepsilon) M_h(\varepsilon) r^A_{eh}(\varepsilon) t^*_{21}(-\varepsilon), && \text{(22c)} \\ S_0^{he}(\varepsilon;t) &= t^*_{12}(-\varepsilon) M_e(\varepsilon) r^A_{he}(\varepsilon) t_{21}(\varepsilon), && \text{(22d)} \end{aligned}$$

where time arguments are omitted on the right hand side of the equations for sake of notation. Multiple reflections between S and F, mediated by propagations through N_2, are described by

$$M_e(\varepsilon) = \left[1 - r^A_{he}(\varepsilon) r_{22}(\varepsilon) r^A_{eh}(\varepsilon) r^*_{22}(-\varepsilon)\right]^{-1}, \tag{23}$$

$$M_h(\varepsilon) = \left[1 - r^A_{eh}(\varepsilon) r^*_{22}(-\varepsilon) r^A_{he}(\varepsilon) r_{22}(\varepsilon)\right]^{-1}. \tag{24}$$

From Eqs. (22), and using $r^A_{eh}(-\varepsilon)^* = r^A_{he}(\varepsilon)$, one obtains the following symmetry relations for the total scattering matrix:

$$\mathcal{S}^{ee}(\varepsilon;t) = \left[\mathcal{S}^{hh}(-\varepsilon;t)\right]^*, \tag{25a}$$

and

$$\mathcal{S}^{eh}(\varepsilon;t) = \left[\mathcal{S}^{he}(-\varepsilon;t)\right]^*. \tag{25b}$$

The frozen scattering matrices in Eqs. (22) are all time-dependent due to the slowly varying magnetization in the ferromagnet. Arguably the easiest way to evaluate the matrix current, is to perform a spinor rotation that aligns the spin quantization axis with the instantaneous magnetization direction.[14,19] The total scattering matrix

$$S_0(\varepsilon;t) = \begin{pmatrix} S_0^{ee} & S_0^{eh} \\ S_0^{he} & S_0^{hh} \end{pmatrix} \tag{26}$$

can be related to the total scattering matrix $\underline{S}$ in the rotating frame by the spinor rotations

$$S_0(\varepsilon;t) = W^\dagger(t) \underline{S}(\varepsilon) W(t), \tag{27}$$

where $W(t) = V(t)U(t)$, with

$$U(t) = \begin{pmatrix} \mathcal{U}(t) & 0 \\ 0 & \mathcal{U}^\dagger(t) \end{pmatrix} = \begin{pmatrix} \exp\left[\frac{\mathrm{i}\Omega t}{2}\sigma^z\right] & 0 \\ 0 & \exp\left[-\frac{\mathrm{i}\Omega t}{2}\sigma^z\right] \end{pmatrix}, \tag{28}$$

and

$$V(t) = \begin{pmatrix} \mathcal{V}(t) & 0 \\ 0 & \mathcal{V}(t) \end{pmatrix} = \begin{pmatrix} \exp\left[\frac{\mathrm{i}\theta(t)}{2}\sigma^y\right] & 0 \\ 0 & \exp\left[\frac{\mathrm{i}\theta(t)}{2}\sigma^y\right] \end{pmatrix}. \tag{29}$$

In the rotating frame, $\underline{S}_0^{ee}$ and $\underline{S}_0^{hh}$ are both diagonal in spin space, while $\underline{S}_0^{eh}$ and $\underline{S}_0^{he}$, which mix spin σ electrons with spin $-\sigma$ holes, only have off-diagonal elements.

Now that the matrix current and relevant scattering matrices are derived, we proceed to study pumped charge and spin currents for a voltage biased trilayer structure.

IV. PUMPED CURRENTS OUT OF EQUILIBRIUM

A complication that arises when the system is driven out of equilibrium, is that time- and energy gradients of the frozen scattering matrix must be evaluated. Before presenting the detailed expressions for charge and spin currents in the normal metal lead, we derive the required gradient corrections. Due to electron-hole symmetry, it is sufficient to consider only A^{he}.

A. Gradient correction matrix

In the following, we determine A^{he} by a formal gradient expansion of the corresponding scattering matrix $\mathcal{S}^{he}$, whose full time and energy dependence of $\mathcal{S}^{he}$ is given by (see Eq. (22d)):

$$\mathcal{S}^{he}(\varepsilon;t) = \left(t^*_{12} \otimes M_e \otimes r^A_{he} \otimes t_{21}\right)(\varepsilon;t). \tag{30}$$

Evaluating the convolutions in the Wigner representation can be done by systematically expanding the exponentials:[20]

$$(A\otimes B)(\varepsilon;t)=\mathrm{e}^{\mathrm{i}(\partial_\varepsilon^A\partial_t^B-\partial_t^A\partial_\varepsilon^B)/2}A(\varepsilon;t)B(\varepsilon;t), \quad (31)$$

where the superscripts indicate which matrix the operator works on. A significant simplification of the final result is achieved when $\Delta\ll\Delta_{xc},E_F$, the regime of interest. Since we are evaluating the energy gradients close to the Fermi level, $\partial_\varepsilon s_F\ll\partial_\varepsilon r^A$, and we obtain the simplified expression

$$\begin{aligned}A^{he}(\varepsilon;t)\approx&-\frac{\mathrm{i}}{2}\partial_\varepsilon\partial_t S_0^{he}+\mathrm{i}t_{12}^*\partial_\varepsilon(M_e r_{he}^A)\partial_t t_{21}\\&+\mathrm{i}t_{12}^*\partial_\varepsilon\partial_t M_e r_{he}^A t_{21}+\mathrm{i}t_{12}^*\partial_t M_e\partial_\varepsilon M_e^{-1}M_e r_{he}^A t_{21}\\&-\mathrm{i}t_{12}^* M_e r_{he}^A\partial_t r_{22}\partial_\varepsilon r_{eh}^A r_{22}^* M_e r_{he}^A t_{21}\\\equiv&-\frac{\mathrm{i}}{2}\partial_\varepsilon\partial_t S_0^{he}+\Gamma^{he}. \quad (32)\end{aligned}$$

for the gradient matrix A^{he}. Here, S_0^{he} is the frozen scattering matrix from Eq. (22d), and Before evaluating the currents, we observe that Γ^{he} in the rotating frame is diagonal in spin space. This fact, which is important when evaluating non-equilibrium pumped charge and spin currents, can be seen from

$$\Gamma^{he}=\mathcal{U}\mathcal{V}^\dagger\underline{\Gamma}^{he}\mathcal{V}\mathcal{U}, \quad (33)$$

with

$$\begin{aligned}\underline{\Gamma}^{he}=&\frac{\mathrm{i}}{2}\underline{t}_{12}^*\partial_\varepsilon(\underline{M}_e r_{he}^A)\Lambda(\underline{t}_{21\uparrow}-\underline{t}_{21\downarrow})\\&+\frac{\mathrm{i}}{2}\underline{t}_{12}^*(\underline{M}_{e\uparrow}-\underline{M}_{e\downarrow})\partial_\varepsilon(r_{he}^A\Lambda\underline{r}_{22}r_{eh}^A)\underline{r}_{22}^*\underline{M}_e r_{he}^A\underline{t}_{21}\\&-\frac{\mathrm{i}}{2}\underline{t}_{12}^*\underline{M}_e r_{he}^A(\underline{r}_{22\uparrow}-\underline{r}_{22\downarrow})\Lambda\partial_\varepsilon r_{eh}^A\underline{r}_{22}^*\underline{M}_e r_{he}^A\underline{t}_{21}\\&-\frac{\mathrm{i}}{2}\underline{t}_{12}^*\partial_\varepsilon(\underline{M}_{e\uparrow}-\underline{M}_{e\downarrow})r_{he}^A\Lambda\underline{t}_{21}, \quad (34)\end{aligned}$$

where

$$\Lambda\equiv\mathcal{V}\mathcal{U}\partial_t(\boldsymbol{m}\cdot\boldsymbol{\sigma})\mathcal{U}^\dagger\mathcal{V}^\dagger=\partial_t\theta\sigma^x+\sin\theta\Omega\sigma^y. \quad (35)$$

Multiplying r_{he}^A, which is $\sim\sigma^y$, with Λ, and using that the other components in the equation are all diagonal, brings us to the conclusion that $\underline{\Gamma}^{he}$ is diagonal in spin space. Finally, we note that $\Gamma^{he}\to 0$ for a vanishing ferromagnetic ordering parameter.

Once the gradient corrections to the frozen scattering matrix are derived, one can obtain non-equilibrium pumped currents to first order in pumping frequency.

B. Pumped charge current

According to Eq. (10), the charge current is obtained by tracing the matrix current (18) over electron-hole, spin and mode space. Making use of the electron-hole symmetries from Eqs. (25a)(25b), and using that both $\mathrm{Tr}\left\{\partial_t S_0^{ee}S_0^{ee\dagger}\right\}=0$ and $\mathrm{Tr}\left\{\partial_t S_0^{he}S_0^{he\dagger}\right\}=0$, one finds that the pumped charge current is determined by

$$\begin{aligned}I_c(t)=\frac{e}{2\pi}\int_{-\infty}^{\infty}\mathrm{d}\varepsilon\,\Big([f_e(\varepsilon)-f_h(\varepsilon)]\,\mathrm{Tr}\Big\{&S_0^{he}S_0^{he\dagger}\\&+A^{he}S_0^{he\dagger}+S_0^{he}A^{he\dagger}-\frac{1}{2}P\left\{S_0^{he};S_0^{he\dagger}\right\}\Big\}\Big), \quad (36)\end{aligned}$$

to first order in pumping parameter frequency. Using that $A^{he}=-\frac{\mathrm{i}}{2}\partial_\varepsilon\partial_t S_0^{he}+\Gamma^{he}$, the current (36) simplifies to

$$\begin{aligned}I_c(t)=\frac{e}{2\pi}\int_{-\infty}^{\infty}\mathrm{d}\varepsilon\,\Big([f_e(\varepsilon)-f_h(\varepsilon)]&\\\times\mathrm{Tr}\Big\{S_0^{he}S_0^{he\dagger}+\Gamma^{he}S_0^{he\dagger}+S_0^{he}\Gamma^{he\dagger}\Big\}\Big). \quad (37)\end{aligned}$$

Any non-equilibrium pumped contributions to the current are determined by the remainder Γ^{he} from Eq. (34). However, as pointed out at the end of Sec. IV A, $\underline{\Gamma}^{he}$ is a diagonal matrix in spin space. From Eq. (22d), we know that $\underline{S}_0^{he}$ is strictly off-diagonal in spin space. This implies that $\mathrm{Tr}\left\{\Gamma^{he}S_0^{he\dagger}\right\}=0$, and the charge current is reduced to the stationary result:

$$I_c=\frac{e}{2\pi}\int_{-\infty}^{\infty}\mathrm{d}\varepsilon\;[f_e(\varepsilon)-f_h(\varepsilon)]\,\tilde{g}(\varepsilon), \quad (38)$$

where the total conductance is defined as

$$\tilde{g}\equiv\sum_{m,n}\left\{\left|\underline{S}_{\downarrow\uparrow,mn}^{he}\right|^2+\left|\underline{S}_{\uparrow\downarrow,mn}^{he}\right|^2\right\}. \quad (39)$$

The result in Eq. (38) shows that there is no pumped charge current in N|F|S structures, even when there is an additional bias voltage driving the system. The stationary result is similar to that obtained in FS|N structures,[19] a result that indicates that the total scattering matrix for a disordered region coupled to a ferromagnetic superconductor, is structurally equivalent to that of a disordered ferromagnetic region coupled to a superconductor. The two structures have different scattering matrices, however, and therefore the expressions for the conductances differ.

C. Pumped spin current

We proceed by evaluating the pumped spin current to first order in pumping parameter frequency. Utilizing the electron-hole symmetry relations for the total scattering matrix, we obtain

$$\boldsymbol{I}_s(t) = \frac{1}{4\pi}\int_{-\infty}^{\infty} \mathrm{d}\varepsilon\ (f_e(\varepsilon) - f_h(\varepsilon))\left[\mathrm{Tr}\left\{\boldsymbol{\sigma}^*\left(S_0^{he}S_0^{he\dagger} + \Gamma^{he}S_0^{he\dagger} + S_0^{he}\Gamma^{he\dagger}\right)\right\} + \partial_\varepsilon \mathrm{ImTr}\left\{\boldsymbol{\sigma}^*\partial_t S_0^{he}S_0^{he\dagger}\right\}\right]$$
$$+ \frac{1}{4\pi}\int_{-\infty}^{\infty} \mathrm{d}\varepsilon\ (-\partial_\varepsilon f_e(\varepsilon))\left[\mathrm{ImTr}\left\{\boldsymbol{\sigma}\partial_t S_0^{ee}S_0^{ee\dagger}\right\} - \mathrm{ImTr}\left\{\boldsymbol{\sigma}^*\partial_t S_0^{he}S_0^{he\dagger}\right\}\right]. \quad (40)$$

Introducing the conductance polarization

$$\tilde{p} \equiv \frac{1}{\tilde{g}}\sum_{m,n}\left\{\left|\underline{S}^{he}_{\downarrow\uparrow,mn}\right|^2 - \left|\underline{S}^{he}_{\uparrow\downarrow,mn}\right|^2\right\}, \quad (41)$$

and the generalized mixing conductance[19]

$$\tilde{g}^{\uparrow\downarrow} \equiv \sum_{m,n}\left\{\delta_{m,n} - \underline{S}^{ee}_{\uparrow,mn}\underline{S}^{ee*}_{\downarrow,mn} + \underline{S}^{he}_{\downarrow\uparrow,mn}\underline{S}^{he*}_{\uparrow\downarrow,mn}\right\}. \quad (42)$$

we find the following expression for the spin current:

$$\boldsymbol{I}_s(t) = -\frac{1}{4\pi}\int_{-\infty}^{\infty} \mathrm{d}\varepsilon\ (f_e(\varepsilon) - f_h(\varepsilon))\left(\tilde{p}\tilde{g}\boldsymbol{m}(t) - \mathrm{Tr}\left\{\boldsymbol{\sigma}^*(\Gamma^{he}S_0^{he\dagger} + S_0^{he}\Gamma^{he\dagger})\right\}\right)$$
$$+ \frac{1}{8\pi}\int_{-\infty}^{\infty} \mathrm{d}\varepsilon\ (f_e(\varepsilon) - f_h(\varepsilon))\partial_\varepsilon\left(\boldsymbol{m}\times\partial_t\boldsymbol{m}\left(\tilde{g} + 2\mathrm{Re}\sum_{m,n}\underline{S}^{he}_{\downarrow\uparrow,mn}\underline{S}^{he*}_{\uparrow\downarrow,mn}\right) + 2\partial_t\boldsymbol{m}\mathrm{Im}\sum_{m,n}\underline{S}^{he}_{\downarrow\uparrow,mn}\underline{S}^{he*}_{\uparrow\downarrow,mn}\right)$$
$$+ \frac{1}{4\pi}\int_{-\infty}^{\infty} \mathrm{d}\varepsilon\ \partial_\varepsilon f_e(\varepsilon)\left(\boldsymbol{m}\times\partial_t\boldsymbol{m}\mathrm{Re}\tilde{g}^{\uparrow\downarrow} + \partial_t\boldsymbol{m}\mathrm{Im}\tilde{g}^{\uparrow\downarrow}\right). \quad (43)$$

The term $\sim \tilde{p}\tilde{g}\boldsymbol{m}(t)$ on the right hand side of Eq. (43) corresponds to the non-equilibrium spin current observed also in the absence of a precessing magnetization vector. Terms in the final line are similar to those derived previously within electro-chemical equilibrium pumping theory for F|N[14], and FS|N structures[19]. However, we ask the reader to note that the generalized mixing conductance in Eq. (3) in Ref. 19 is valid for triplet superconductors only; the correct mixing conductance for a singlet superconductor is given by Eq. (42) above. The remaining terms on the right hand side of Eq. (43) are non-equilibrium, pumped contributions to the spin current. They depend on pumping parameter frequency via $\partial_t\boldsymbol{m}$ and the Λ term from Eq. (35), which is contained in the gradient remainder Γ^{he}.

Finally, we would like to point out that there are no pumped contributions to the *longitudinal* spin current $I_s^{||} \equiv \boldsymbol{m}\cdot\boldsymbol{I}_s$. The terms in the second and third line of Eq. (43) are all perpendicular to $\boldsymbol{m}$, so this leaves only a possible gradient remainder contribution coming from Γ^{he}. However, due to the particular matrix structure of Γ^{he} mentioned in Sec. IV A, $\boldsymbol{m}\cdot\mathrm{Tr}\{\boldsymbol{\sigma}^*\Gamma^{he}S_0^{he\dagger}\}$ is traceless in spin space. This observation implies that, when $\Delta \ll \Delta_{xc}, E_F$, the longitudinal spin current is stationary and unaffected by the precessing magnetization. Thus, to first order in precession frequency:

$$I_s^{||} = \boldsymbol{m}(t)\cdot\boldsymbol{I}_s(t) = -\frac{1}{4\pi}\int_{-\infty}^{\infty} \mathrm{d}\varepsilon\,(f_e(\varepsilon) - f_h(\varepsilon))\tilde{p}\tilde{g}. \quad (44)$$

In the following, we will investigate pumped charge and spin currents when the ferromagnetic region is longer than the typical transverse spin coherence length.

D. Long ferromagnet limit

When the length L_x of the ferromagnet is longer than the transverse spin coherence length,

$$L_x > L_{sc} \equiv \frac{\pi}{k_{F\uparrow} - k_{F\downarrow}}, \quad (45)$$

where $k_{F\sigma}$ is the Fermi wave vector of a spin σ electron, we expect to find a mixing conductance that is determined by the properties of the N|F subsystem, characterized by the spin-dependent conductances[14]

$$g^{\sigma\sigma'} = \sum_{m,n}\left(\delta_{m,n} - \underline{r}_{\sigma,mn}\underline{r}^*_{\sigma',mn}\right). \quad (46)$$

Indeed, in the limit (45), one can disregard "mixing transmission" terms, $\sum_{m,n}\underline{t}_{\sigma,mn}\underline{t}^*_{-\sigma,mn} \to 0$, so that

$\sum_{m,n} \underline{S}^{he}_{\downarrow\uparrow,mn} \underline{S}^{he*}_{\uparrow\downarrow,mn} \to 0$. Disregarding interference terms between reflected and transmitted electronic wave functions, one obtains

$$\sum_{m,n} \underline{S}^{ee}_{\uparrow,mn} \underline{S}^{ee*}_{\downarrow,mn} \to \sum_{m,n} \underline{r}_{11\uparrow,mn} \underline{r}^{*}_{11\downarrow,mn}, \tag{47}$$

for a long ferromagnet. This implies that $\tilde{g}^{\uparrow\downarrow} \to g^{\uparrow\downarrow}$, while the total conductance $\tilde{g}$ and the conductance polarization $\tilde{p}$ remain unchanged. Since the mixing conductance is now determined by properties of the N|F structure, energy gradients of the mixing conductance should be disregarded in the limit $\Delta \ll \Delta_{xc}, E_F$, as described in Sec. IV A. Finally, by an explicit calculation, one can show that $\mathrm{Tr}\{\Gamma^{he} S_0^{he\dagger} \boldsymbol{\sigma}^*\} \sim \underline{t}_{\sigma} \underline{t}^{*}_{-\sigma}$, which vanishes when Eq. (45) holds. To summarize, when the ferromagnet is longer than the transverse spin coherence length, the charge current and longitudinal spin current are still given by

$$I_c = \frac{e}{2\pi} \int_{-\infty}^{\infty} \mathrm{d}\varepsilon \; (f_e(\varepsilon) - f_h(\varepsilon))\, \tilde{g}, \tag{48}$$

and

$$I_s^{||} = -\frac{1}{4\pi} \int_{-\infty}^{\infty} \mathrm{d}\varepsilon \; (f_e(\varepsilon) - f_h(\varepsilon)) \tilde{p}\tilde{g}, \tag{49}$$

while the transverse spin current is simplified to

$$\boldsymbol{I}_s^{\perp}(t) = \frac{1}{8\pi} \int_{-\infty}^{\infty} \mathrm{d}\varepsilon \; (f_e(\varepsilon) - f_h(\varepsilon)) \boldsymbol{m} \times \partial_t \boldsymbol{m} \partial_\varepsilon \tilde{g} + \frac{1}{4\pi} \int_{-\infty}^{\infty} \mathrm{d}\varepsilon \; \partial_\varepsilon f_e(\varepsilon) \left(\boldsymbol{m} \times \partial_t \boldsymbol{m} \mathrm{Re} g^{\uparrow\downarrow} + \partial_t \boldsymbol{m} \mathrm{Im} g^{\uparrow\downarrow} \right). \tag{50}$$

With no applied bias voltage, the pumped spin current in Eq. (50) is identical to that found in N|F systems[14], as should be expected. In this situation, emission of spins from the ferromagnet into the normal metal are unaffected by the superconductor.

To compare the exact result (43) with the long ferromagnet approximation of Eq. (50), we plot in Fig. 2 the spin current along $\partial_t \boldsymbol{m}$ for a ballistic N|F|S trilayer, as a function of the ratio between the ferromagnet length (L_x) and the transverse spin coherence length (L_{sc}) defined in Eq. (45). When $L_x \leq L_{sc}$, non-negligible "mixing transmission" terms combine with energy gradients of the scattering matrix and produce large deviations between the two equations. As L_x exceeds L_{sc}, the fit improves and the exact result oscillates towards the spin current obtained by the approximate Eq. (50). These numerical results suggest that, indeed, structure added to the transverse spin current by scattering matrix energy gradients and "mixing transmission" terms are most important for ferromagnets with lengths shorter than, or approximately equal to, the transverse spin coherence length.

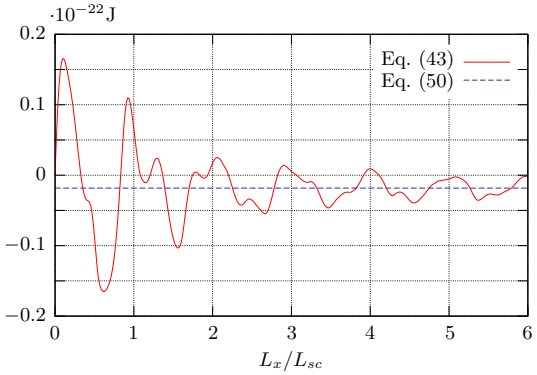

(a) Transverse spin component $\partial_t \boldsymbol{m} \cdot \boldsymbol{I}_s/\Omega$

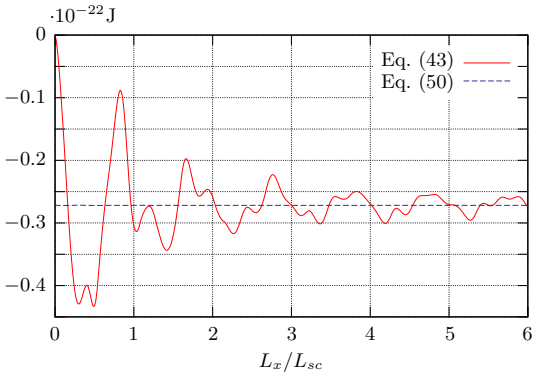

(b) Transverse spin component $(\boldsymbol{m} \times \partial_t \boldsymbol{m}) \cdot \boldsymbol{I}_s/\Omega$

FIG. 2: Exact (red line) and approximate (blue dashed line) transverse spin currents for a ballistic N|F|S structure as functions of length of the ferromagnetic region. In the plot, $E_F = 10$ eV, $\Delta_{xc} = 9E_F/16$, $\Delta = E_F/160$, $eV = \Delta/2$ and $\Omega = 0.2$ GHz. The straight black lines serve as guides to the eye, and indicate the non-zero values the currents oscillate toward.

V. CONCLUSION

In conclusion, we have derived non-equilibrium pumped charge and spin currents to first order in pump frequency, using time-dependent scattering theory. Magnetization precession induces transverse spin currents, but neither charge nor longitudinal spin currents, which are both given by their stationary values. The currents are expressed in terms of generalized, spin dependent conductances, that include spin-dependent scattering in the ferromagnet and Andreev reflection at the F|S interface. Finally, we consider trilayers where the ferromagnetic region is longer than the transverse spin coherence length, and derive an approximate expression for the transverse spin current. Numerical calculation of the spin current in a ballistic trilayer shows good agreement between exact and approximate spin currents for ferromagnets whose

layer thicknesses exceed the transverse spin coherence length.

Acknowledgments

This work was supported in part by the Research Council of Norway, Grants Nos. 158518/143 and 158547/431.

[1] K. Kawaguchi and M. Sohma, Phys. Rev. B **46**, 14722 (1992).
[2] E. A. Demler, G. B. Arnold, and M. R. Beasley, Phys. Rev. B **55**, 15174 (1997).
[3] M. Giroud, H. Courtois, K. Hasselbach, D. Mailly, and B. Pannetier, Phys. Rev. B **58**, R11 872 (1998).
[4] V. T. Petrashov, I. A. Sosnin, I. Cox, A. Parsons, and C. Troadec, Phys. Rev. Lett. **83**, 3281 (1999).
[5] R. S. Keizer, S. T. B. Goennenwein, T. M. Klapwijk, G. Miao, and A. Gupta, Nature **439**, 825 (2006).
[6] F. S. Bergeret, A. F. Volkov, and K. B. Efetov, Phys. Rev. Lett. **86**, 4096 (2001).
[7] A. Kadigrobov, R. I. Shekhter, and M. Jonson, Europhys. Lett. **54**, 394 (2001).
[8] F. S. Bergeret, A. F. Volkov, and K. B. Efetov, Rev. Mod. Phys. **77**, 1321 (2005).
[9] G. Tkachov, E. McCann, and V. I. Fal'ko, Phys. Rev. B **65**, 024519 (2001).
[10] S. Takahashi, S. Hikino, M. Mori, J. Martinek, and S. Maekawa, Phys. Rev. Lett. **99**, 057003 (2007).
[11] M. Houzet, Phys. Rev. Lett. **101**, 057009 (2008).
[12] J. C. Slonczewski, J. Magn. Magn. Mater. **159**, L1 (1996).
[13] L. Berger, Phys. Rev. B **54**, 9353 (1996).
[14] Y. Tserkovnyak, A. Brataas, G. E. W. Bauer, and B. I. Halperin, Rev. Mod. Phys. **77**, 1375 (2005).
[15] S. Mizukami, Y. Ando, and T. Miyazaki, J. Magn. Magn. Mater. **226-230**, 1640 (2001).
[16] C. Bell, S. Milikisyants, M. Huber, and J. Aarts, Phys. Rev. Lett. **100**, 047002 (2008).
[17] J. P. Morten, A. Brataas, G. E. W. Bauer, W. Belzig, and Y. Tserkovnyak, Europhys. Lett. **84**, 57008 (2008).
[18] M. A. Sillanpää, T. T. Heikkilä, R. K. Lindell, and P. J. Hakonen, Europhys. Lett. **56**, 590 (2001).
[19] A. Brataas and Y. Tserkovnyak, Phys. Rev. Lett. **93**, 087201 (2004).
[20] J. Rammer and H. Smith, Rev. Mod. Phys. **58**, 323 (1986).
[21] M. Büttiker, Phys. Rev. B **46**, 12485 (1992).
[22] A. Brataas, G. E. W. Bauer, and P. J. Kelly, Phys. Rep. **427**, 157 (2006).
[23] M. Büttiker, H. Thomas, and A. Prêtre, Z. Phys. B **94**, 133 (1994).
[24] P. W. Brouwer, Phys. Rev. B **58**, R10 135 (1998).
[25] M. Büttiker and M. Moskalets, *Scattering Theory of Dynamic Electrical Transport* (Springer-Verlag Berlin, 2006), vol. 690 of *Lect. Notes Phys.*, p. 33.
[26] A. F. Andreev, Zh. Eksp. Teor. Fiz. **46**, 1823 (1964), [Sov. Phys. JETP **19**, 1228 (1964)].
[27] C. W. J. Beenakker, Phys. Rev. B **46**, 12841 (1992).
[28] J. B. Ketterson and S. N. Song, *Superconductivity* (Cambridge University Press, 1999).
[29] M. G. Vavilov, V. Ambegaokar, and I. L. Aleiner, Phys. Rev. B **63**, 195313 (2001).
[30] M. Blaauboer, Phys. Rev. B **65**, 235318 (2002).
[31] B. Wang and J. Wang, Phys. Rev. B **66**, 125310 (2002).
[32] B. Wang and J. Wang, Phys. Rev. B **66**, 201305 (2002).
[33] Y. Tserkovnyak and A. Brataas, Phys. Rev. B **64**, 214402 (2001).
[34] M. Moskalets and M. Büttiker, Phys. Rev. B **69**, 205316 (2004).
[35] X. Waintal and P. W. Brouwer, Phys. Rev. B **65**, 054407 (2002).